

# Development of a Non-Reacting LES Solver for Unstructured Grid

Anoop Sam Abraham

ME17MTECH11026

A Thesis Submitted to  
Indian Institute of Technology Hyderabad  
In Partial Fulfillment of the Requirements for  
The Degree of Master of Technology



भारतीय प्रौद्योगिकी संस्थान हैदराबाद  
Indian Institute of Technology Hyderabad

Department of Mechanical and Aerospace Engineering

June 2019

## Declaration

I declare that this written submission represents my ideas in my own words, and where ideas or words of others have been included, I have adequately cited and referenced the original sources. I also declare that I have adhered to all principles of academic honesty and integrity and have not misrepresented or fabricated or falsified any idea/data/fact/source in my submission. I understand that any violation of the above will be a cause for disciplinary action by the Institute and can also evoke penal action from the sources that have thus not been properly cited, or from whom proper permission has not been taken when needed.



\_\_\_\_\_  
(Signature)

\_\_\_\_\_  
(Anoop Sam Abraham)

ME17MTECH11026

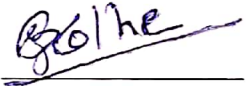
(Roll No.)

## Approval Sheet

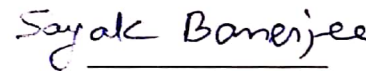
This Thesis entitled Development of a Non-Reacting LES Solver for Unstructured Grid by Anoop Sam Abraham is approved for the degree of Master of Technology from IIT Hyderabad.



(Dr. Vinod Janardhanan) Examiner  
Dept. of Chemical Eng  
IITH



(Dr. Pankaj Kohle) Examiner  
Dept. of Mechanical Eng  
IITH



(Dr. Sayak Banerjee) Examiner  
Dept. of Mechanical Eng  
IITH



(Prof. Raja Banerjee) Adviser  
Dept. of Mechanical Eng  
IITH

## Acknowledgements

I was able to complete the thesis work successfully due to the unconditional assistance and support from a few people. Firstly, I would like to express my sincere gratitude towards my thesis adviser Prof. Raja Banerjee for believing in me and providing the opportunity to work on turbulence modelling. Throughout the course of the thesis work, his interest in me and his exemplary guidance have always motivated me to think beyond conventional ways and explore new ideas.

The research group of my thesis adviser consists of three young and enthusiastic students who have greatly assisted me in understanding the concepts in Openfoam and ICEMCFD. I would like to wholeheartedly thank Kumar Mayank, Krishnakant and Keerthi Santhosh Kumar for sharing their knowledge and experiences with me.

Last but not the least, I would like to thank my friends in IIT Hyderabad for making my two years as a Masters Student truly memorable. I would also acknowledge the love and support provided by my family throughout this endeavor.

# Dedication

*To my brother...*

## Abstract

The present thesis consists of development of an LES based explicit solver which could simulate non reacting flows. The numerical simulation is carried out using Dynamic k equation subgrid scale model. Along with solving the Navier- Stokes equation a convection diffusion equation for mass fraction is also solved which would correct the equivalent density. The length and time scales for the mesh and simulations are calculated based on the Kolmogorov's hypothesis and the CFL number is calculated accordingly. An explicit solver is used because of the fact that the calculated CFL number is extremely lower than 1.

Two cases were validated using the above developed code, first is the case of an axisymmetric turbulent jet of air entering a quiescent atmosphere and the second one is the case where a variable density fluid (here Helium) entering the same quiescent air. The development of the plumes are captured. The development of the plume structures of both the cases are discussed. The averaged velocity profiles are also discussed. The mean velocity, turbulent fluctuations and Reynolds stresses are plotted. A brief study on the parallelisation technique used in OpenFoam is also done. Finally using the fluctuating data from both simulations the energy spectrum graphs are plotted which ensures that the mesh is suitable for the present study.

# Contents

Declaration . . . . .	ii
Approval Sheet . . . . .	iii
Acknowledgements . . . . .	v
Abstract . . . . .	vii
<b>List of Figures</b>	<b>4</b>
<b>List of Tables</b>	<b>5</b>
<b>Nomenclature</b>	<b>6</b>
<b>1 Introduction</b>	<b>9</b>
<b>2 Turbulent Jets</b>	<b>12</b>
2.1 Turbulent Jets . . . . .	12
2.2 Laminar and Turbulent Flows . . . . .	14
2.3 Numerical Methods . . . . .	15
2.3.1 Direct Numerical Simulation . . . . .	16
2.3.2 LES . . . . .	17
2.3.3 RANS . . . . .	20
2.4 Reynolds Averaged Approach vs. LES . . . . .	21
2.5 Effect of Grid Sensitivity on SGS LES models . . . . .	22
2.6 Literature Review . . . . .	23
<b>3 Computational Model</b>	<b>28</b>
3.1 Governing Equation and Discretization . . . . .	28
3.1.1 Finite Volume Method . . . . .	30
3.1.2 Governing Equations . . . . .	31
3.1.3 Finite Volume Discretization . . . . .	31
3.1.4 Explicit Algorithm . . . . .	33

---

3.1.5	Boundary Conditions . . . . .	35
3.2	Problem Definition . . . . .	36
3.3	Parallel Computing . . . . .	37
3.3.1	SMAC Algorithm . . . . .	40
<b>4</b>	<b>Results and Discussion</b>	<b>41</b>
4.1	Computational Grid . . . . .	41
4.2	Air in quiescent atmosphere . . . . .	43
4.3	Running Parallel Applications . . . . .	48
4.4	Helium into quiescent atmosphere . . . . .	50
4.5	CoVo Test . . . . .	56
<b>5</b>	<b>Conclusions and Future Scops</b>	<b>60</b>
	<b>References</b>	<b>61</b>



# List of Figures

2.1	Jet with Reynolds number $10^5$ (Picture courtesy : Steven Crow and Cambridge University Press [1]) . . . . .	13
2.2	Axisymmetric Turbulent jets (Photograph courtesy : Steven Crow and Cambridge University Press[1]) . . . . .	13
2.3	Plane turbulent plume showing large scale motions [1] . . . . .	15
2.4	Experimental setup [2] . . . . .	24
3.1	A finite control volume (non-moving) [3] . . . . .	30
3.2	Schematic diagram of boundary conditions . . . . .	36
3.3	Computational Domain with geometric parameters. . . . .	37
4.1	Computational Grid for air case . . . . .	42
4.2	Computational grid with for helium case . . . . .	42
4.3	Mass fraction development of air jet at various time . . . . .	43
4.4	Mean Velocity profile . . . . .	44
4.5	Axial Mean Velocity profile in the radial direction . . . . .	45
4.6	Velocity variation with time at (0,0.3,0) . . . . .	45
4.7	Axial Turbulent intensity variation in the radial direction . . . . .	46
4.8	Radial and Azimuthal Turbulent intensity variation in the radial direction	46
4.9	Axial Turbulent intensity variation in the radial direction . . . . .	47
4.10	Energy Spectrum . . . . .	47
4.11	(a)Time vs No. of processors plot(b)Actual vs Theoretical Speed up plot	49
4.12	Mass fraction development of helium jet at various time . . . . .	51
4.13	Mean velocity profile in the radial direction . . . . .	52
4.14	Variation of velocity at (0,0.5,0) . . . . .	53
4.15	Velocity profile in the radial direction . . . . .	53
4.16	Mean velocity profile in the radial direction . . . . .	54
4.17	Radial and Azimuthal Turbulent intensity variation in the radial direction	54

4.18 Reynolds stress variation across the helium jet . . . . .	55
4.19 Energy Spectrum . . . . .	56
4.20 Geometry for CoVo test . . . . .	57
4.21 Boundary Condition for CoVo test . . . . .	58
4.22 (a)Initial condition for $U_x$ (b)Initial condition for Pressure . . . . .	58
4.23 $U_x$ image after $30\frac{L}{U}$ s . . . . .	59
4.24 Plot of velocity in the y direction to x . . . . .	59

# List of Tables

3.1 Case Details . . . . .	37
----------------------------	----

# Nomenclature

## Roman Symbols

$c_p$	Specific heat at constant pressure
$C_v$	Total specific heat at constant volume
$c_v$	Specific heat at constant volume
$E$	Total specific energy
$\mathbf{F}$	Vector of convection fluxes
$\mathbf{G}$	Vector of diffusion fluxes
$H$	Total specific enthalpy
$k$	Turbulent kinetic energy
$k_f$	Thermal conductivity of fluid
$M$	Mach number
Ma	Mach Number
$P$	Pressure
$Pr$	Prandtl number
$\mathbf{R}$	Vector of residuals
$R$	Specific gas constant
$\mathbf{S}_w$	Vector of source fluxes
$T$	Temperature
$u$	Velocity component in the X direction
$v$	Velocity component in the Y direction
$V_n$	Contra-variant velocity
$\mathbf{W}$	Vector of conservative variables

$w$  Velocity component in the Z direction

### Greek Symbols

$\Delta t$  Time-step size

$\epsilon$  Turbulent dissipation

$\Gamma$  Pre-conditioning matrix

$\gamma$  Ratio of specific heats

$\mu$  Dynamic viscosity of fluid

$\omega$  Turbulent specific dissipation

$\rho$  Density of the fluid

$\tau$  Normal/shear stress

$\theta$  Work done by viscous stresses

### Other Symbols

$\oint_S$  Integration over a surface  $S$

$\int_V$  Integration over a volume  $V$

### Acronyms / Abbreviations

AMD Advanced Micro Devices

AUSM Advection Upstream Splitting Method

CFD Computational Fluid Dynamics

CFL Courant-Friedrichs-Lewy

CGNS CFD General Notation System

CPU Central Processing Unit

CUDA Compute Unified Device Architecture

DNS Direct Numerical Simulation

FRANS Favre- and Reynolds-Averaged Navier-Stokes

FVM Finite Volume Method

GPU Graphics Processing Unit

HPF High-Performance Fortran

LES Large Eddy Simulation

MIMD Multiple-Instruction Multiple-Datastream

MPI	Message Passing Interface
NACA	National Advisory Committee for Aeronautics
NASA	National Aeronautics and Space Administration
PDE	Partial Differential Equation
RAM	Random Access Memory
RANS	Reynolds-Averaged Navier-Stokes
SA	Spalart Allmaras
SIDS	Standard Interface Data Structures
SISD	Single-Instruction Single-Datastream
SLAU	Simple Low-dissipation AUSM
SST	Shear Stress Transport

# Chapter 1

## Introduction

Literally combustion means burning of something. Combustion produces energy. It forms more than 85 percent of the energy produced on earth at present. From the growing demand we can predict that the energy of the future will be also taken from combustion as the demand is increasing even faster than the supply. So it is necessary for combustion science to extract the energy without wasting fuel, increasing pollution, killing people and changing the climate. Also combustion is the major source of pollution now a days. Noise pollution, which is a big after effect of combustion is a major pollutant. Also fire safety is a very important topic of discussion these days. It is notable to state that in Canada from 1993 to 2002 there were 600,000 fire accidents happened [4]. Therefore fire modelling is such an important field in prevention and determining optimal fire safety designs. Fires can be modeled to determine the extent of damages that may occur in defined situations, as well as to assess probable fire risks which may arise. This can be achieved through experimental or numerical methods. The study of non-reacting buoyant plumes is an important step in understanding the convective transport of fluids and is useful in fire modeling.

Climate changes occur due to the emissions from combustion. Role of  $CO_2$  in climate change is the talking point these days, which again is an after effect of combustion. Contrails which are formed after the wake of aircrafts make a major air pollutant in the sky. Thus the importance of investigation of combustion is of high importance. It is necessary to investigate and understand combustion from an engineering viewpoint. With more insight about combustion we can find how it affects the earth and its livelihood.

The study of non-reacting buoyant jets forms an important step in understanding the convective transport of fluids and is useful in modeling flamelets. In situations

where the prediction of fire spreading rates and overall smoke plume dynamics are desired, and values for combustion rate and chemical components are not necessary, the simulation can be simplified and cost can be reduced by modeling a non-reacting buoyant plume with an equivalent Schmidt number. The reason is that the hot combustion products resulting from a flame will be having similar flow dynamics to that of a buoyant plume. So modelling buoyant plume forms the best substitution in the modeling of flames in combustion.

One of the best methods for flow simulations is achieved using Computation Fluid Dynamics. Computational Fluid Dynamics (CFD) is a branch of fluid mechanics which solves Partial Differential Equations on a fluid flow numerically using computers. CFD solvers are used now a days to predict flow patterns across components which vary from nano-scale levels like chipsets to an entire spacecraft. It is also used for predicting flow patterns on the weather over the earth. At present CFD plays an important role in aerospace and automobile industries and helps in saving millions of money which were spent earlier for testing and manufacturing prototypes . It acts as a channel between the complex fluid flows and speed computing.

The present work uses Finite Volume Method (FVM), where the domain of interest is divided into a number of smaller volumes (cells), thus forming a mesh. The solution is obtained at the centers of these cells by discretizing the partial differential equations. In FVM we approximate the solution on each volume as the value at the centroid. Similar approximations are made on each cell. Because of this approximation it is required to have a large number of cells, so in fact very small cell sizes.

The present thesis involves the discussion of an explicit solver which was developed which can be used to simulate non-reacting buoyant plumes. Chapter 2 deals with the CFD studies where turbulence models are discussed and how it is implemented in OpenFoam Software. This chapter deals with a few approaches in CFD used in simulating turbulent flows. The chapter provides details of experimental works which are done using turbulence models. Also it discusses about DNS , LES and RANS models. The present aim of the thesis work is also discussed in the chapter.

Two cases are studies, one non- buoyant flow which involves the LES simulation of air in quiescent air and buoyant flow which is the helium in quiescent air case. The governing equations along with the discretization of the convection flux and diffusion flux terms are discussed in chapter 3.

Chapter 4 presents the results and further discussion which involves the compar-



ison of the computational results with the experimental results. The dependency of computational results are examined and it is compared with similar works done in past. Chapter 5 involves the future work which can be done using the work which has been done.

# Chapter 2

## Turbulent Jets

This chapter describes the importance of turbulence in buoyant flow jets. The energy cascading is explained as if how the energy is transferred from large scales eddies to the dissipative scales. The Kolmogorov hypotheses is used to explain the isotropic motion of the dissipative scales. The various turbulence models are explained in this chapter along with numerical methods. This then leads to literature review where we discuss on axisymmetric jets are done, thus the evolution to the present study is done. After this the aim of the present thesis work is done with detailed explanation of the problem. Here we will discuss the two cases which are part of the thesis that is the air in air case which is the non buoyant case and the helium in air case which is the buoyant jet case.

### 2.1 Turbulent Jets

Before we attempt complex flows it is always better to model less complicated but similar flows. Thus keeping that in mind the turbulent round jets are a very good case which can be modelled before attempting complex flow jets. Rodi[1] differentiates three different types of flow which are turbulent : turbulent jets, turbulent plumes and turbulent buoyant jets or forced plumes. In turbulent jets the only source of momentum flux and kinetic energy for the motion of fluid is the pressure drop through the orifice. Thus an outward momentum is created which forces the jet to move outwards from the orifice. Vortex structures are also formed which aids to the momentum growth of the turbulent jets. An example of a turbulent jet is shown in the figure 2.1

The images shows the turbulent jets. As can be seen from the images the larger

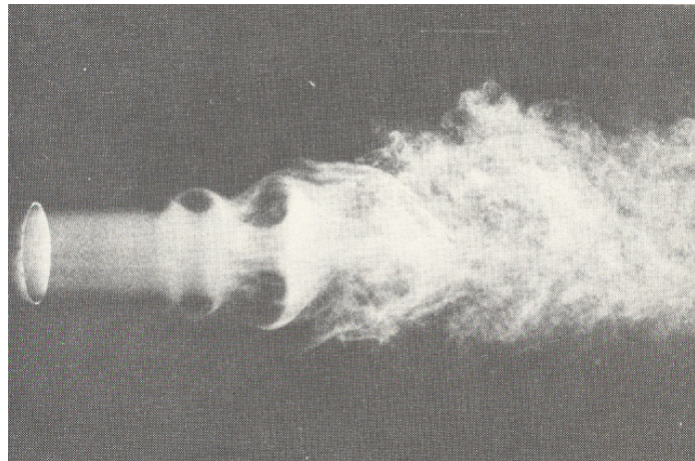


Figure 2.1: Jet with Reynolds number  $10^5$  (Picture courtesy : Steven Crow and Cambridge University Press [1])

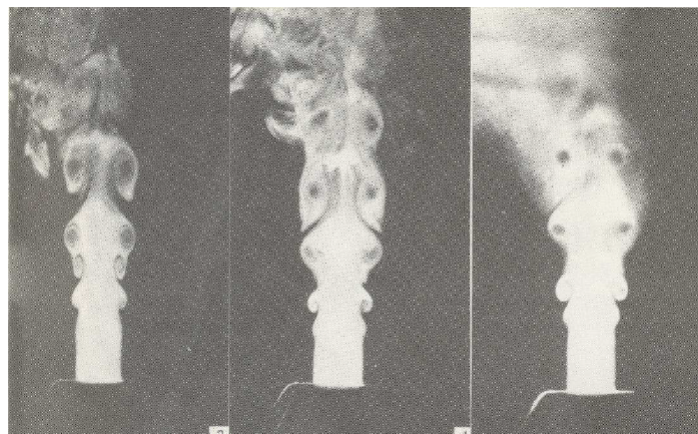


Figure 2.2: Axisymmetric Turbulent jets (Photograph courtesy : Steven Crow and Cambridge University Press[1])

eddies break up into smaller eddies. Eventually a turbulent plume is developed when the primary source of momentum flux and kinetic energy is the gravitational force. All the characteristics and behaviours are affected by the buoyancy flux which is actually the rate of production of mass deficiency. Turbulent jets makes a transition into a plume because of the effect of buoyancy. As a result when the motion is majorly depending on the mass deficiency rather than the initial momentum flux, the jet forms a plume structure as it majorly depends on the gravitational force.

## 2.2 Laminar and Turbulent Flows

In fluid study, laminar flow is when the fluid particles follows smooth paths in layers, with each layer moving smoothly past the adjacent layers with very little where as turbulent flows are characterized by fluctuating pressure and flow velocities. Turbulent flows are unsteady and irregular in nature. It contains different scales of motion. This eventually leads to a velocity field with a different variation in characteristics in both time and space. Chaotic flows are a phenomenon which happens in turbulent flows. Turbulent flows are commonly observed in day to day phenomenons like briskly flowing water bodies, storm clouds, or smoke from a cigarette or a chimney, and most of the fluid flows which are occurring in nature or created by engineering phenomenons are turbulent.

One of the examples of turbulent flows is the buoyancy driven flow. Turbulence is created by buoyancy of the fluid plume rising in the quiescent air and thus, it is very important to understand the turbulent flow dynamics.

Turbulent fluid flows consist of rotational flow structures, known as eddies, in a range of length scales. The length scales can vary from the characteristic length of the flow to a really smaller length scale. The larger length scales of motion predominately transport the conserved properties and they dependent on the initial conditions and boundary conditions whereas the smaller length scales of motions are statistically independent flow therefore isotropic in nature. It was Richardson[5] who introduced the concept of flow through an energy cascade. He described how turbulent kinetic energy is transferred and how the energy is distributed. The turbulent kinetic energy is extracted from the mean flow when it interacts with the macro scale eddies. Subsequently this energy is transferred from the larger eddies due to breakup of larger eddies to the smaller eddies. Finally when the eddies are small enough to interact with the viscous scale this energy is dissipated as viscous heat dissipation.

It was Kolmogorov[6] who introduced the concept of the smallest length and time scales. The large length scale flow motions are very much dependent on the mean flow. The directional dependence decreases as the length scale value decreases. Thus, the small length scale motion becomes statically independent of the geometry and are universal in nature. So it can be assumed that the small scale motions in all turbulent flow are similar. It only depends on the energy transfer and viscous effects.



Figure 2.3: Plane turbulent plume showing large scale motions [1]

The Kolmogorov turbulent length scale is given by,

$$\frac{\eta}{L} = Re_t^{-\frac{3}{4}} \quad (2.1)$$

and the time scale is given by,

$$\frac{\tau}{t} = Re_t^{-\frac{1}{2}} \quad (2.2)$$

The energy spectrum function,  $E(k)$ , describes the turbulent kinetic energy distribution among the various sized eddies. The energy spectrum forms the relation between energy density per unit wave number 'E', wave number 'k' and the dissipation rate, 'e'. By Kolmogorov's hypothesis the energy spectrum is defined as:

$$E(k) = Ce^{2/3}k^{-5/3} \quad (2.3)$$

Here C is a constant. This energy spectrum is very important in modeling approaches.

## 2.3 Numerical Methods

Experiments for understanding the turbulent jets is extremely costly and time consuming as it requires high definition equipments to capture the turbulent parameters. Computational Fluid Dynamics (CFD) plays a very important role in modeling these flows which can capture the flow dynamics. In CFD turbulence modelling is classified as Direct Numerical Simulation (DNS), Large Eddy Simulation (LES) and Reynolds-

Averaged Navier-Stokes (RANS). This section describes each approach and how they are implemented.

### 2.3.1 Direct Numerical Simulation

DNS is the most accurate approach to turbulence simulation. The Navier-Stokes equations are solved directly without any modelling techniques. In DNS all the flow is captured as such so it demands a wide range of resolutions for the grids and it makes it computationally very expensive.

In order to obtain the characteristic of the largest eddy the computational domain should be several times larger than their eddy sizes. The computational cost of DNS modeling a cubic domain depends on the length of the domain  $L$  the grid spacing  $\Delta x$ , and the time step  $\Delta t$ . The grid spacing depends on the size of the dissipative scales which are to be resolved. The time step should be of the order of the Kolmogorov time scale. Additionally for a time accurate solution, the time step must be such that the fluid parcel shall not move more than one grid spacing per one time step. The number of total cells and the time step actually depend on the Reynolds number. The dependency of the number of grid nodes on Reynold's number is given by,

$$N \propto Re^{\frac{3}{4}} \quad (2.4)$$

So the total number of grid points is given by,

$$N \propto Re^{\frac{9}{4}} \quad (2.5)$$

Time step is dependent on grid spacing through the CFL number and the turbulent kinetic energy.

Good results are obtained if the time scale is of the order of the kolmogorov's time scale,  $k/\epsilon$ , So the total number of time steps is given by,

$$M = \frac{4\tau}{\Delta t} \propto Re^{3/4} \quad (2.6)$$

So the number of grid points as well as the number of time steps drastically increases as the flow becomes turbulent that is the reynolds number becomes so high. Therefore DNS is very much limited to very low reynolds number and that too in very simple geometries. It is clear from the above discussion that DNS is computa-

tionally very expensive. At the present computer technology DNS is computationally expensive.

### 2.3.2 LES

Large Eddy Simulation is based on philosophy that the larger length scales depend on the initial conditions and boundary conditions and the smaller length scales are isotropic in nature. The large scale eddies are resolved and models are used for the smaller scales. Consequently LES requires coarser grid compared to DNS. Computational costs are significantly reduced while using LES when compared with DNS.

A filtering operation is done so as to separate the larger scale with the smaller scale based on a particular reference scale. In this process it filters the eddies whose length scales are smaller than the filtering grid spacing or width used in the computations. The dynamics of the large eddies will be then governed by this resolved governing equations.

The filtered variable ( $\bar{\phi}$ ) is defined by

$$\bar{\phi}(x) = \int_D \phi(x') G(x, x') dx' \quad (2.7)$$

Here  $G(x, x')$  is the filter kernel.

Now the  $\phi$  field will be the sum of the residual component,  $u'(x, t)$ , and the filtered component,  $\bar{\phi}(x, t)$ .

Now the filtered Navier Stokes equations and the mass conservation equation will be as follows,

$$\frac{\partial \rho}{\partial t} + \frac{\partial}{\partial x_i} (\rho u_i) = 0 \quad (2.8)$$

$$\frac{\partial}{\partial t} (\rho \bar{u}_i) + \frac{\partial}{\partial x_j} (\rho \bar{u}_i \bar{u}_j) = \frac{\partial}{\partial x_j} (\sigma_{ij}) - \frac{\partial p}{\partial x_i} - \frac{\partial \tau_{ij}}{\partial x_j} \quad (2.9)$$

The stress tensor is defined by,

$$\sigma_{ij} = \mu \left( \frac{\partial \bar{u}_i}{\partial x_j} + \frac{\partial \bar{u}_j}{\partial x_i} \right) - \frac{2}{3} \mu \frac{\partial \bar{u}_i}{\partial x_i} \delta_{ij} \quad (2.10)$$

Here  $\tau_{ij}$  is the subgrid scale stress which is given by,

$$\tau_{ij} = \rho \bar{u}_i \bar{u}_j - \rho \bar{u}_i \bar{u}_j \quad (2.11)$$

After the filtering operation, it is required to model the subgrid scale stresses. Here  $\mu_{sgs}$  is the subgrid scale turbulent viscosity. The isotropic part of the subgrid-scale stresses  $\tau_{kk}$  is not modeled, but added to the filtered static pressure term.  $\bar{S}_{ij}$  is the rate-of-strain tensor for the resolved scale defined by

$$\bar{S}_{ij} \equiv \frac{1}{2} \left( \frac{\partial \bar{u}_i}{\partial \bar{x}_j} + \frac{\partial \bar{u}_j}{\partial \bar{x}_i} \right) \quad (2.12)$$

For compressible flows a different approach is used, and it is not discussed as the present work deals with incompressible flows.

### Smagorinsky-Lilly Model

This is the simplest model which is known as the eddy viscosity model[7].

$$\mu_{sgs} = \rho L_s^2 |\bar{S}| \quad (2.13)$$

where  $L_s$  is the mixing length for subgrid scales and  $|\bar{S}| \equiv \sqrt{2\bar{S}_{ij}\bar{S}_{ij}}$ .  $L_s$  is calculated by,

$$L_s = \min(\kappa d, C_s \Delta) \quad (2.14)$$

where  $\kappa$  is the von Kármán constant,  $d$  is the distance to the closest wall,  $C_s$  is the Smagorinsky constant, and  $\Delta$  is the local grid scale.  $\Delta$  is computed according to the volume of the computational cell using,

$$\Delta = V^{1/3} \quad (2.15)$$

Lilly[8] obtained 0.17 as a value for  $C_s$  for isotropic homogeneous turbulence in the inertial subrange. However, this value was found to cause excessive damping of large-scale fluctuations in the presence of mean shear and in transitional flows as near solid boundary, and has to be reduced in such regions. As a conclusion,  $C_s$  can't be used as a universal constant, which has been a shortcoming of this model. Nonetheless  $C_s$  value of 0.1 is used to yield good results for a wide range of flows.

### Dynamic Smagorinsky-Lilly Model

Germano et al. and subsequently Lilly[9] developed a method where by the Smagorinsky constant,  $C_s$ , is dynamically computed based on the data available from the mo-



tion of the resolved scales. The dynamic approach removes the need to provide the constant  $C_s$  in the beginning.

The dynamic procedure applies a second filter (called the test filter) to the equations of motion. This new filter width  $\hat{\Delta}$  will be equal to twice the grid filter width  $\Delta$ . these filters provide a resolved flow field. The contribution from small scale filters will be in between the test filter and grid filter. Using these information the model constant is formulated. The variable density formulation of this model is explained below.

At the test filtered field level, the SGS stress tensor can be expressed as:

$$T_{ij} = \widehat{\rho u_i u_j} - (\widehat{\rho u_i u_j} \widehat{\rho u_j} / \widehat{\rho}) \quad (2.16)$$

Both  $T_{ij}$  and  $\tau_{ij}$  are modeled the same way with as Smagorinsky-Lilly model, assuming scale similarity,

$$\tau_{ij} = -2C\bar{\rho}\Delta^2\tilde{S}|\tilde{S}_{ij} - \frac{1}{3}\tilde{S}_{kk}\delta_{ij}) \quad (2.17)$$

$$T_{ij} = -2C\widehat{\rho}\widehat{\Delta}^2|\tilde{S}|(\tilde{S}_{ij} - \frac{1}{3}\widehat{S}_{kk}\delta_{ij}) \quad (2.18)$$

The grid filtered SGS[10] and the test-filtered SGS are related by the Germano identity such that,

$$L_{ij} = T_{ij} - \widehat{\tau}_{ij} = \widehat{\rho u_i u_j} - \frac{1}{\widehat{\rho}}(\widehat{\rho u_i} \widehat{\rho u_j}) \quad (2.19)$$

Where  $L_{ij}$  is computed from the resolved large eddy field. Substituting the grid filter Smagorinsky-Lilly model and Equation the following expressions is derived for solving C,

$$C = \frac{(L_{ij} - L_{kk}\delta_{ij}/3)}{M_{ij}M_{ij}} \quad (2.20)$$

### Dynamic Kinetic Energy Subgrid-Scale Model

The Smagorinsky and dynamic Smagorinsky-Lilly models are generally algebraic models in which subgrid-scale stresses are parameterized using the resolved velocity scales. The assumption is that local equilibrium between the transferred energy through the grid-filter scale and the dissipation of kinetic energy at small subgrid scales. The subgrid-scale turbulence modeled better by solving for the subgrid-scale turbulence kinetic energy. The model is proposed by Kim and Menon. The subgrid-scale kinetic

energy is defined as,

$$k_{\text{sgs}} = \frac{1}{2} \left( \overline{u_k^2} - \bar{u}_k^2 \right) \quad (2.21)$$

The subgrid-scale eddy viscosity,  $\mu_t$ , is computed using  $k_{\text{sgs}}$  as,

$$\mu_T = C_k k_{\text{sgs}}^{1/2} \Delta_f \quad (2.22)$$

where  $\Delta_f$  is the filter-size computed from  $\Delta_f \equiv V^{1/3}$ .

The subgrid-scale stress can then be written as,

$$\tau_{ij} - \frac{2}{3} k_{\text{sgs}} \delta_{ij} = -2C_k k_{\text{sgs}}^{1/2} \Delta_f \bar{S}_{ij} \quad (2.23)$$

$k_{\text{sgs}}$  is obtained by solving its transport equation,

$$\frac{\partial \bar{k}_{\text{sgs}}}{\partial t} + \frac{\partial \bar{u}_j \bar{k}_{\text{sgs}}}{\partial x_j} = -\tau_{ij} \frac{\partial \bar{u}_i}{\partial x_j} - C_\epsilon \frac{k_{\text{sgs}}^{3/2}}{\Delta_f} + \frac{\partial}{\partial x_j} \left( \frac{\mu_t}{\sigma_k} \frac{\partial k_{\text{sgs}}}{\partial x_j} \right) \quad (2.24)$$

In the above equations, the model constants,  $C_k$  and  $C_\epsilon$ , are determined dynamically.

### 2.3.3 RANS

Reynolds Averaged Navier Stokes approach(RANS)[11] decomposes the Navier Stokes Equation into mean and fluctuating components. For velocity,

$$u_i = \bar{u}_i + u'_i \quad (2.25)$$

where  $\bar{u}_i$  and  $u'_i$  are the mean and fluctuating velocity components.

Substituting expressions of this form for the flow variables into the instantaneous continuity and momentum equations and taking a time (or ensemble) average (and dropping the overbar on the mean velocity,  $\bar{u}$ ) yields the ensemble-averaged momentum equations. They can be written in Cartesian tensor form as:

$$\frac{\partial \rho}{\partial t} + \frac{\partial}{\partial x_i} (\rho u_i) = 0 \quad (2.26)$$

$$\frac{\partial}{\partial t} (\rho u_i) + \frac{\partial}{\partial x_j} (\rho u_i u_j) = -\frac{\partial p}{\partial x_i} + \frac{\partial}{\partial x_j} \left[ \mu \left( \frac{\partial u_i}{\partial x_j} + \frac{\partial u_j}{\partial x_i} - \frac{2}{3} \delta_{ij} \frac{\partial u_k}{\partial x_k} \right) \right] + \frac{\partial}{\partial x_j} (-\rho \overline{u'_i u'_j}) \quad (2.27)$$

This is the averaged Navier Stokes equation. They have the same general form

as the instantaneous Navier-Stokes equations, with the velocities and other solution variables now representing time-averaged values. Additional terms now appear that represent the effects of turbulence.

## 2.4 Reynolds Averaged Approach vs. LES

Resolving all the length scales for obtaining the flow parameters of high Reynolds number flows and in complex geometries is not practically possible at this time. The available methods to render Navier-Stokes equations are Reynolds averaging and sub-grid filtering approach. These methods will have additional terms in the governing equations that need to be modeled in order to achieve "closure" for the unknowns [12].

In Reynolds averaged Navier-Stokes (RANS), all the range of turbulent scales are modelled. This approach uses the transport of the average flow parameters. Till recently engineering applications used RANS approach due to comparatively less computational cost. The typical closure models are Spalart-Allmaras,  $k-\epsilon$  and its variants,  $k-\omega$  and its variants, and the Reynolds Stress Model (RSM). In RANS the unsteadiness are externally imposed or self sustained flows require time dependent boundary conditions or transient sources or providing flow instabilities like vortex shedding.

LES is another approach in which the large eddies are solved (computed) in a time dependent simulation using filtered Navier Stokes equations. Modelling component is less in LES which eventually reduces the errors which arises in turbulent flows. It is also believed to be easier to find a "universal" model for the small scales, since they tend to be more isotropic and less affected by the macroscopic features like boundary conditions, than the large eddies. Filtering is definitely a mathematical approach done on Navier-Stokes equations to remove the eddies that are smaller than the size of the filter. Like RANS, after filtering is done in Navier Stokes equation, additional unknown terms are to be modelled in order to achieve the closure. Statistics of time varying flow fields like time averages and rms values of the solution variables, which are of engineering interest, can be obtained while computing the time dependent simulation.

As the Reynolds number increases the resources which are required for computation also increases significantly. This is mainly because of the need to accurately resolve the energy-containing turbulent eddies in both space and time domains, which

becomes most acute in near-wall regions where the scales to be resolved eddies become much smaller. Wall functions in combination with a coarse near wall mesh can be employed, often with some success, to reduce the cost of LES for wall-bounded flows. However, one needs to carefully consider the ramifications of using wall functions for the flow in question. For the same reason (to accurately resolve the eddies), LES also requires highly accurate spatial and temporal discretizations.

## 2.5 Effect of Grid Sensitivity on SGS LES models

In Large Eddy Simulation (LES), turbulent flows are studied by resolving large scales of motion and modelling the smaller scales using the help of a Subgrid Scale (SGS) models which employs an eddy viscosity assumption to model the SGS stresses. In Smagorinsky model the Smagorinsky constant is assumed as a fixed value for the entire domain and for every time step. However it was not valid for all the cases. As the flow configurations change the value of the Smagorinsky constant should also change. This fact was considered by Germano et al. [10] to calculate the Smagorinsky constant based on the flow field information in their Dynamic model. Even with the dynamically calculated Smagorinsky constant, there were certain inherent limitations in the model. The velocity scale which was chosen used in the model avoids it from predicting the eddy viscosity at the regions where vorticity levels are much higher than the irrotational strain. The eddy viscosity in the near wall region is over predicted due to large values of the velocity gradient which is a major drawback since all the turbulent fluctuations and consequently the eddy viscosity should vanish near the wall.

The Wall Adapting Local Eddy Viscosity (WALE) model, improves the limitations of the Smagorinsky model [13]. In the WALE model it uses a velocity scale for the eddy viscosity calculations which indeed predicts more accurate eddy viscosity values in high vorticity regions and areas where irrotational strains are high. Though the wall adapting models seem to overcome the limitations of Smagorinsky model, LES for a flow with high Reynolds number is computationally prohibitive if the wall is being resolved completely. One method which can reduce the computational cost is to use RANS-LES hybrid models where RANS is used in the near wall regions and LES is used in the core region [14]. Another approach is to use Large Eddy Simulations in conjunction with the wall models. The wall model creates a profile which is smooth

for eddy viscosity from the wall up to the first grid point which lies in the logarithmic region[15].

The choice of the grid for LES is critical. In RANS simulations a grid convergence test is employed and the chosen grid offers no major improvements in the results after refining the grid further. Such a method will not be feasible with LES firstly because of the computational restrictions. Secondly, as the LES grid is further refined, the contribution of the SGS model shifts towards smaller scales until the LES converges to DNS. The accuracy of the LES is inhibited by many factors such as the numerical errors and the modeling errors which usually interact with each other[16]. It is extremely difficult to separate numerical errors with modeling errors which make grid independence test in LES very difficult[16] [17]. But there are specific quality parameters which show that the grids taken for LES are done with less errors. This enables us to test the prediction of various SGS models on relatively coarser grids associated with complex geometries while minimizing the errors. One of the parameters which check the suitability of the grid is the energy spectrum.

The energy spectrum function [18],  $E(k)$ , describes the turbulent kinetic energy distribution among the various sized eddies. The energy spectrum forms the relation between energy density per unit wave number 'E', wave number 'k' and the dissipation rate, 'e'. By Kolmogorov's hypothesis the energy spectrum is defined as:

$$E(k) = Ce^{(2/3)}k^{-5/3} \quad (2.28)$$

Here C is a constant. In the present work the energy spectrum diagram is plotted for the meshes to check the suitability of LES simulations in the meshes used instead of the grid independence tests.

## 2.6 Literature Review

In this section the researches which were done on axisymmetric jets are done. This includes both the experimental works and computational works. Computational works are mostly done by using the methods which were discussed in the above section that is the RANS and the LES methods. The recent advancement in the computer technology allows research on turbulent jets using large eddy simulations and much accurate results are obtained.

The present work has been inspired from the work done by Panchapakesan AND

Lumley[2], where they have done a study on axisymmetric turbulent jet of air. A turbulent round jet of air discharging into quiescent air was studied experimentally. Hot wire probes mounted on a moving shuttle were used to eliminate rectification errors due to flow reversals in the intermittent region of the jet. In the paper measurements were made in an air jet of diameter 6.1 mm at a Reynolds number of 11000 are reported. The experimental setup is shown in the figure 2.4.

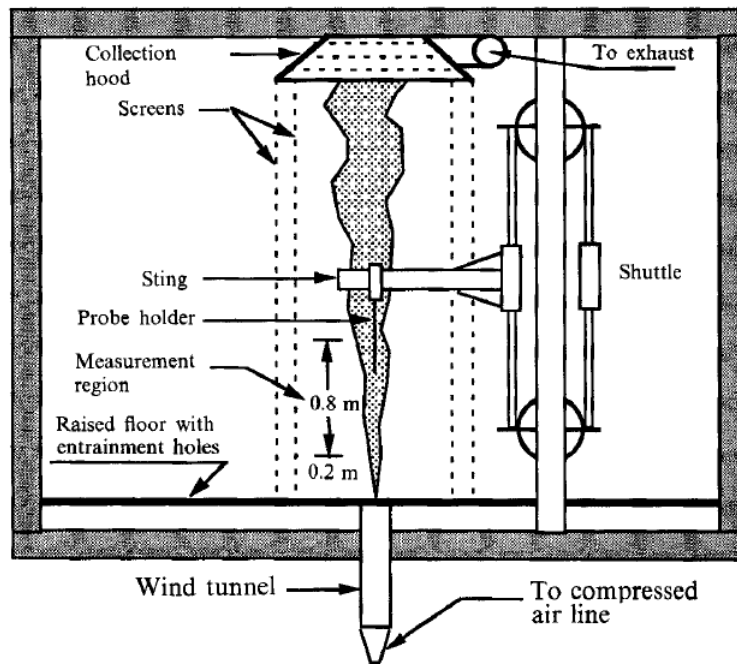


Figure 2.4: Experimental setup [2]

The exit velocity of the jet was checked using a pressure transducer and it was maintained within  $\pm 0.05\%$  of the desired velocity. The turbulent intensity was maintained of the order of 2%. In the work the velocity profile in the radial direction and the turbulent fluctuations in the axial and radial directions are measured and documented. Also the Reynolds stress were plotted. Moments of velocity fluctuations up to fourth order were measured to characterize turbulent transport in the jet and to evaluate current models for triple moments that occur in the Reynolds stress equations. The following conclusions were done from the above experiment,

The values of turbulent intensities on the axis in the paper are significantly lower than those of W & F, Rodi, CHG-LDA and CHG-SHW, all of which were made in jets with a Reynolds number of  $10^5$  whereas the present Reynolds number is  $10^4$ . Values reported by Browne et al. in the near field ( $x/d = 15$ ) for a jet of Reynolds number

$1.77 \times 10^4$  concur with the present measurements at  $x/d = 30$ .

An extension of the work is also by the same team using a buoyant jet. Here they considered the Helium jet [19] which is ten times lighter than that of air. With the same set up instead of air, helium jet is allowed to flow into the quiescent air. The flow facility is the same as explained in the above setup. Here the Schmidt number is taken to be 0.7. The jet discharge Froude number was  $1.4 \times 10^4$  and the measurement range was in the intermediate region between the non-buoyant jet region and the plume region. In this experiment also the velocity profile and the turbulent parameters which were mentioned above were measured and plotted. Higher order moments were also measured and plotted in the paper. The following conclusions were obtained using this study.

The mean velocity decays along the axial direction. This indicates a density ratio dependence that is different from that suggested by the effective diameter. Both velocity and concentration fields are seen to approach the scaling for the plume in the far field. Due to the mean momentum added due to buoyancy the radial velocity profile is wider than that of the air in air turbulent jet case. The concentration fields and spreading rates of the mean velocity shows a turbulent Schmidt number of 0.7, which agrees with other measurements of scalars in round jets. Significant increase in turbulent intensity is obtained in this experiment in comparison to the non buoyant jet. The origin of these higher values is believed to be near the nozzle inlet but in the study that area was not investigated.

It was McGrattan et al. [20] who stated that because of the requirements of numerous parameters for turbulence in CFD turbulence modelling, and also these values will be different for different applications accuracy of turbulence models be case specific. They attempted large eddy simulation to simulate large eddies using a constant value for eddy viscosity to model the effect of the small scale eddies. The experiment was conducted to have an assessment of temperature and velocity predictions on smoke movement in an enclosed fire. Results were well predicted and it matched with the experimental results. In the end they concluded that wide range of similar works can be done using Large eddy simulations.

Ma and Quintiere [21] studied fire plumes which are axisymmetric attempting to extend the work of McGrattan et al. from isolated fire plumes to unconfined fires. They did the simulation using Large eddy simulation having the value of Smagorinsky constant value as 0.2. Test cases consisted of a free burning pool fire. The predicted

flame heights matched with the flame height relations. Temperature and velocity predictions were also done but the results were over predicted.

Zhou et al.[22] did a study on non reacting buoyant jets using large eddy simulations . They found out that majority of the works on turbulent jets had been done on predicting the flow variables in the far-field regions. Nearby the source of the jets the laminar to turbulent transitions take place and large vortex structures are formed at those areas. These vortex structures lead to the puffing cycles observed in fire plumes [39] as well as break down to small scale vortices in the plume. Zhou et al. did the study on buoyant jets which had various density ratios. The Smagorinsky constant was taken as 0.1 for the smaller eddies and the predicted puffing cycle was matching with the experimental data near the source region. The mean velocity along the centerline axis from the plume source indicated that the plume gas initially accelerates due to the buoyancy forces and then decelerates as turbulent mixing takes place. The initial acceleration is very much dependent on the density ratio of the surrounding ambient air to the gas  $\frac{\rho_1}{\rho_2}$ . The density ratio also affects the spreading rates of the velocity and temperature. An increase in density ratio increases the spreading rates due to a high increase in turbulence intensity in the flow.

Zhou et al. then applied LES on reacting plumes after their study on non reacting plumes. Similar to non-reacting buoyant jet case the reacting jet case showed large vortex structures nearer to the source region. The large vortices brake down into small scale eddies after the transition from laminar to turbulent flows. The results obtained were then validated with the experimental results. The velocity profile, temperature profile, mixture fraction were very well predicted.

O'Hern et al.[23] and DesJardin et al.[24] were able to study the near field of a large turbulent helium plume using experiments. LES simulations were done to determine flow dynamics and plume instabilities , including velocity profiles and mass concentration, as a function of grid resolution as well as how the results react with and without the use of the SGS model. The finest mesh gave the best results indicating the limitation of SGS model. It was found that for buoyancy driven flows, the SGS model is not sufficient. Time averaged and rms values for the plume concentration were found to be significantly over predicted near the plume base and very sensitive to the grid resolution. And again rms velocity(streamwise) error rised as distance was increased from the plume source.

RANS approach has been widely used for the study of turbulent jets. It was in



2015 Kannan [25] reported results using the RANS simulation based on the work done by Lumley and panchapakeshan[2]. There he has used the RANS  $k - \epsilon$  model and obtained satisfactory results for the velocity profile.

RANS method is used widely for the modelling of turbulent plumes. The  $k - \epsilon$  turbulence model of Launder and Spalding[26] is commonly applied to close the Navier-Stokes equations[27]. This model is the most popular due to its easy approach, robustness and documented validation test cases. However, well known deficiencies in the standard formulation of the model include the under prediction of the spreading rate of vertical thermal plumes and the over prediction of the spreading rate of horizontal stratified flows [28].

In order to avoid the buoyancy deficiency in the standard  $k - \epsilon$  model, Algebraic Stress Model(ASM) is used. It has the potential to better model the buoyancy and rotational effects because it accounts for Reynolds stress anisotropy but is more computationally expensive than the  $k - \epsilon$  model and has not been as widely validated. It was Davidson [29] who suggested a hybrid model between the  $k - \epsilon$  model and ASM. The non-isotropic Reynolds stress due to buoyancy is taken from the ASM and the remaining is modeled using the  $k - \epsilon$  model with the Simple Gradient Diffusion Hypothesis (SGDH) used to model the production of turbulence due to buoyancy. Upon testing their model on a thermal plume, it was found that there was very little difference in predicted velocity and heat transfer rates between the  $k - \epsilon$  model and the hybrid model. Use of the hybrid model increased the CPU time by only 3%.

# Chapter 3

## Computational Model

The present work involves the development of an explicit solver that can simulate highly turbulent buoyancy driven shear flows. This chapter deals with the present problem which describes the domain and mesh which were used in the simulation. Also the mathematical formulation of Navier-Stokes equation is also described in detail. The governing equations and the discretized equations are discussed. The studies mentioned in the previous discussion are used in the formulation of the code in openFoam. Here in the present work LES based turbulent model is chosen for both the air and helium cases. The dynamic k equation sub grid scale model is used in the simulation of both the cases. The velocity profile, turbulent intensity values and the Reynolds stress values are all compared and validated using the experimental data available from Panchapakshian and Lumley[2] paper. The schematic diagram of the present thesis work has been given in the ??.

### 3.1 Governing Equation and Discretization

Fluid dynamics stands for the investigation of interactive motion of a large number of fluid particles, which are atoms and molecules. They are governed by three basic conservation laws of physics which are:

1. the conservation of mass,
2. the conservation of momentum, and
3. the conservation of energy.

In fluid dynamics, the density of any fluid is assumed to be high enough so that it can be approximated as a *continuum*, which means even an infinitesimally small volume element is made up of a sufficient number of particles. The three conservation laws applied to inviscid flows are represented mathematically by the Euler equations. Viscous stresses are included in these to form PDEs known as the Navier-Stokes equations. The energy equation is derived from the first law of thermodynamics to solve for the temperature distribution across a domain. The full set of Navier-Stokes equations and the energy equation in the three dimensions form a system of non-linear second order PDEs. Analytical solutions exist only for a few simple cases which are one/two dimensional or axi-symmetric. This makes the application of numerical solution techniques inevitable and led to the development of computational fluid dynamics.

The continuum assumption allows the specification of mean velocity and mean kinetic energy for any finite volume fluid element, which implies that velocity, pressure, temperature, density and other important quantities can be defined at any point in the fluid. In Computational Fluid Dynamics(CFD), researchers employ the Finite Volume Method(FVM) to solve a discretized form of the complete set of Navier-Stokes equations over any computational domain divided into a number of smaller volumes. In this method, the conservation of a certain flow variable/property means that its net variation inside any arbitrary control volume is expressed as the net effect of three quantities:

1. the amount of the property being transported across the boundaries(flux),
2. the effect of internal forces and sources, and
3. the effect of external forces acting on the volume.

The conservation of an arbitrary vector  $\mathbf{U}$  across a finite control volume shown in figure 3.1 is expressed as

$$\frac{\partial}{\partial t} \int_V \mathbf{U} dV + \oint_S [(\mathbf{F}_C - \mathbf{F}_D) \cdot \hat{n}] dS = \int_V \mathbf{S}_W dV + \oint_S [\mathbf{S}_S \cdot \hat{n}] dS, \quad (3.1)$$

where,  $\mathbf{F}_C$  and  $\mathbf{F}_D$  represent the convective flux and diffusion flux tensors respectively, and  $\mathbf{S}_W$  and  $\mathbf{S}_S$  denote the volume source and surface source tensors respectively. This integral form of the conservation law remains valid even in the presence of discontinuities in the flow-field like shocks and contact discontinuities.

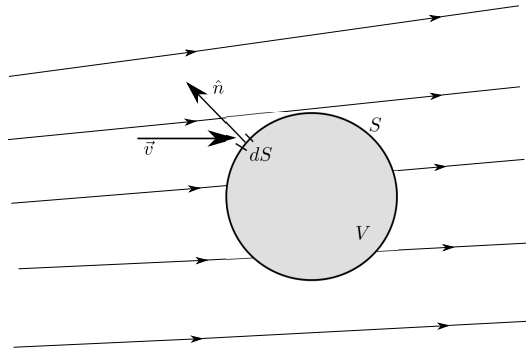


Figure 3.1: A finite control volume (non-moving) [3]

The conservation laws of mass, momentum and energy applied over a finite control volume results in the complete set of Navier-Stokes equations in the integral form which is to be discretized to obtain its numerical solution. The details of the derivation of the conservation laws and their application over a control volume can be found in any advanced fluid dynamics textbook[30][31].

### 3.1.1 Finite Volume Method

The most commonly used methods to discretize any governing equation which are,

- Finite Difference Method (FDM)
- Finite Element Method (FEM)
- Finite Volume Method (FVM)

Among them, FDM uses the equation in it's differential form where as FEM and FVM uses the equations in their weaker forms or integral forms. The compiled solver utilizes OpenFOAM libraries that involve discretization using the finite volume method. Many of the commercially available codes use FVM as the preferred choice of discretization. It is because of the following reasons:

- It is easier to implement
- It provides a more natural treatment of Neumann boundary conditions as well as that of discontinuous source terms due to their reduced requirements on the regularity or smoothness of the solution.
- It suits better to deal with complex geometries in multidimensional problem as the integral formulations do no rely on any special mesh structure.

### 3.1.2 Governing Equations

In the present cases we have used turbulence under consideration. LES model has been used. The Dynamic k equation sub grid scale model has been used in the present study. The following equations forms the governing equations for the case which we study.

The mass conservation equation is given by,

$$\frac{\partial \rho}{\partial t} + \frac{\partial}{\partial x_i}(\rho u_i) = 0 \quad (3.2)$$

The filtered Navier Stokes equation is given by,

$$\frac{\partial(\rho \bar{u}_i)}{\partial t} + \frac{\partial(\rho \bar{u}_i \bar{u}_j)}{\partial x_j} = -\frac{\partial \bar{p}}{\partial x_i} + \frac{\partial \bar{\tau}_{ij}}{\partial x_j} \quad (3.3)$$

In the above equation  $\rho$  is the density and  $g$  is the acceleration due to gravity.

Also there is a convection diffusion equation for mass fraction which is given by,

$$\frac{\partial y}{\partial t} + U \cdot \nabla y = \nabla(D_{12} \nabla y) \quad (3.4)$$

Here  $y$  is the mass fraction and  $D_{12}$  is the mass diffusion coefficient.

Once the value of  $Z$  is obtained for each cell the density is corrected as follows,

$$\rho_{eq.} = y * \rho_1 + (1 - y) * \rho_2 \quad (3.5)$$

For capturing the turbulence we have used the dynamic k equation sub grid model in LES. So the k equation is given by,

$$\frac{\partial \bar{k}_{sgs}}{\partial t} + \frac{\partial \bar{u}_j \bar{k}_{sgs}}{\partial x_j} = -\tau_{ij} \frac{\partial \bar{u}_i}{\partial x_j} - C_\epsilon \frac{\bar{k}_{sgs}^{3/2}}{\Delta_f} + \frac{\partial}{\partial x_j} \left( \frac{\mu_{sgs}}{\sigma_k} \frac{\partial \bar{k}_{sgs}}{\partial x_j} \right) \quad (3.6)$$

In the above equations, the model constants,  $C_k$  and  $C_\epsilon$ , are determined dynamically and  $\sigma_k$  is hardwired to 1.0.

### 3.1.3 Finite Volume Discretization

The equations mentioned above are in differentiable form . The finite volume discretization needs the equations to be in their integral form. In order to convert the equations to it's integral form volume integration is performed over a control volume.

Mathematically,

$$\iiint_V \frac{\partial \rho}{\partial t} + \nabla \cdot (\rho U \otimes U) = \iiint_V -\nabla P + \Delta(\mu \nabla U) dV + \rho g \nabla V \quad (3.7)$$

Here we are neglecting the surface tension forces.

The above equation can be split into four terms based on their contribution to flow:

1. Temporal term
2. Convective term
3. Diffusion term
4. Pressure term
5. Source term due to body forces

The nomenclature used here for discretization will be as follows: In unstructured grids 'p' is the present cell and 'nb' is the neighbouring cell. n and n+1 stand for current and next time step respectively.

#### Temporal term

$$\iiint_V \frac{\partial U}{\partial t} dV = V_p \frac{V_p^{n+1} - V_p^n}{\Delta t} \quad (3.8)$$

here  $V_p$  is the volume of cell under consideration. The basic assumption is that the volume of a cell remain constant throughout  $\Delta t$ . For the other terms Gauss divergence theorem is used to convert volume integral into surface integral. According to Gauss divergence theorem we have,

$$\iiint_V \nabla \cdot \phi dV = \iint_A \phi \cdot \bar{n} dV \quad (3.9)$$

In pure physical sense Gauss Divergence theorem can be thought of as a result that relates flow of a vector field through a surface to the behaviour of a vector field inside the surface.

#### Convective term

$$\iiint_V \nabla \cdot (U \otimes U) dV = \sum_f U_f S_f \quad (3.10)$$

Here  $U_f$  is the velocity of the face under consideration.  $S_f$  is the face area.

#### Diffusion term

$$\iiint_V \nabla \cdot (\mu \nabla U) dV = \sum_f \mu \nabla U_f \cdot dS_f \quad (3.11)$$

here  $S_f$  is the area vector normal to f face.

#### Pressure Term

$$\iiint_V \nabla P dV = \sum_f P_f S_f \quad (3.12)$$

$P_f$  is the pressure at the face center and  $S_f$  as explained above.

### 3.1.4 Explicit Algorithm

The final discretized equation of Navier- Stokes equation is given by,

$$V_p \frac{U_p^{n+1} - U_p^n}{\Delta t} + \sum_f U_f^n F_f^n + \sum_f F_{fdu}^n = -\frac{1}{\rho} \sum_f P_f^{n+1} S_{fx} + V_p \rho g \quad (3.13)$$

$$V_p \frac{V_p^{n+1} - V_p^n}{\Delta t} + \sum_f V_f^n F_f^n + \sum_f F_{fdu}^n = -\frac{1}{\rho} \sum_f P_f^{n+1} S_{fy} + V_p \rho g_i \quad (3.14)$$

$$V_p \frac{W_p^{n+1} - W_p^n}{\Delta t} + \sum_f W_f^n F_f^n + \sum_f F_{fdu}^n = -\frac{1}{\rho} \sum_f P_f^{n+1} S_{fz} + V_p \rho g_i \quad (3.15)$$

These are the momentum equations in the 3 directions.

The continuity equation is given by,

$$\sum_f F_f = 0 \quad (3.16)$$

The working of the explicit algorithm is explained as follows,

1. Obtaining the initial guessed velocities by dropping the pressure terms. This is the predictor step.
2. The continuity equation is imposed using the predicted velocities obtained from

the predictor step.

3. Using the pressure values obtained corrected velocities are obtained.

Predictor step: The pressure terms are ignored in the above equations as follows,

$$V_p \frac{U_p^* - U_p^n}{\Delta t} + \sum_f U_f^n F_f^n + \sum_f F_{fdu}^n = V_p \rho g_i \quad (3.17)$$

$$V_p \frac{V_p^* - V_p^n}{\Delta t} + \sum_f V_f^n F_f^n + \sum_f F_{fdu}^n = V_p \rho g_i \quad (3.18)$$

$$V_p \frac{W_p^* - W_p^n}{\Delta t} + \sum_f W_f^n F_f^n + \sum_f F_{fdu}^n = V_p \rho g_i \quad (3.19)$$

Subtracting these equations from the above equations will obtain,

$$V_p \frac{U_p^{n+1} - U_p^*}{\Delta t} = -\frac{1}{\rho} \sum_f P_f^{n+1} S_{fx} \quad (3.20)$$

$$V_p \frac{V_p^{n+1} - V_p^*}{\Delta t} = -\frac{1}{\rho} \sum_f P_f^{n+1} S_{fy} \quad (3.21)$$

$$V_p \frac{W_p^{n+1} - W_p^*}{\Delta t} = -\frac{1}{\rho} \sum_f P_f^{n+1} S_{fz} \quad (3.22)$$

Using the continuity equation and giving the values of  $U_p^{n+1}$ ,  $V_p^{n+1}$  and  $W_p^{n+1}$  we obtain the pressure poisson equation as,

$$\frac{\Delta t}{\rho} \nabla^2 P_f = \nabla U_f^* \quad (3.23)$$

Once the value of  $P^{n+1}$  is obtained we find the velocity corrections. Finally we add the corrected velocities to the predicted velocity values as,

$$U_p^{n+1} = U_p^* + U_p' \quad (3.24)$$

$$V_p^{n+1} = V_p^* + V_p' \quad (3.25)$$

$$W_p^{n+1} = W_p^* + W_p' \quad (3.26)$$



Now that the velocities are known these values are used in the convection diffusion equation of mass fraction. The discretized form is given by,

$$V_p \frac{y_p^{n+1} y_p^n}{\Delta t} + \sum_f F_f^n y^n = D_{12} \sum_f F_{fdy}^n \quad (3.27)$$

$y^n$  values are known from the initial condition or from the previous time step. And hence the value of  $y^{n+1}$  can be obtained.

After obtainig the value of Z for each cell, the density is corrected as follows,

$$\rho_{eq.} = y * \rho_1 + (1 - y) * \rho_2 \quad (3.28)$$

### 3.1.5 Boundary Conditions

The schemaic of the boundary conditions is given in the following figure 3.2. Here in both the air and helium cases same boundary conditions are used as both the experiments were done in similar conditions and with the same setup by Lumley and Panchapakeshan[2][19].

#### Inlet

A neumann boundary condition for pressure and a Dirichlet boundary condition for the velocity. The inlet velocity in the air in air case is given as 27m/s and for the helium in air case it is specified as 72.5m/s. The turbulent intensity value is given for the inlet as 2%. Also the mass fraction value is taken to be 1.

#### Wall

A no slip boundary condition is applied at the walls and a zero gradient condition is applied for the pressure.

#### Z- Entrainment

Z- Entrainment is the faces where the area is normal to the z-axis. Here a zero shear boundary condition is specified using a mixed boundary condition.

#### X- Entrainment

X- Entrainment is the faces where the area is normal to the x-axis. Here a zero shear boundary condition is specified using a mixed boundary condition.

#### Outlet

A Neumann boundary condition is applied for velocity at the outlet and a Dirichlet

boundary condition is applied for pressure. Zero gradient boundary condition is applied for velocity and atmospheric pressure is given for the pressure.

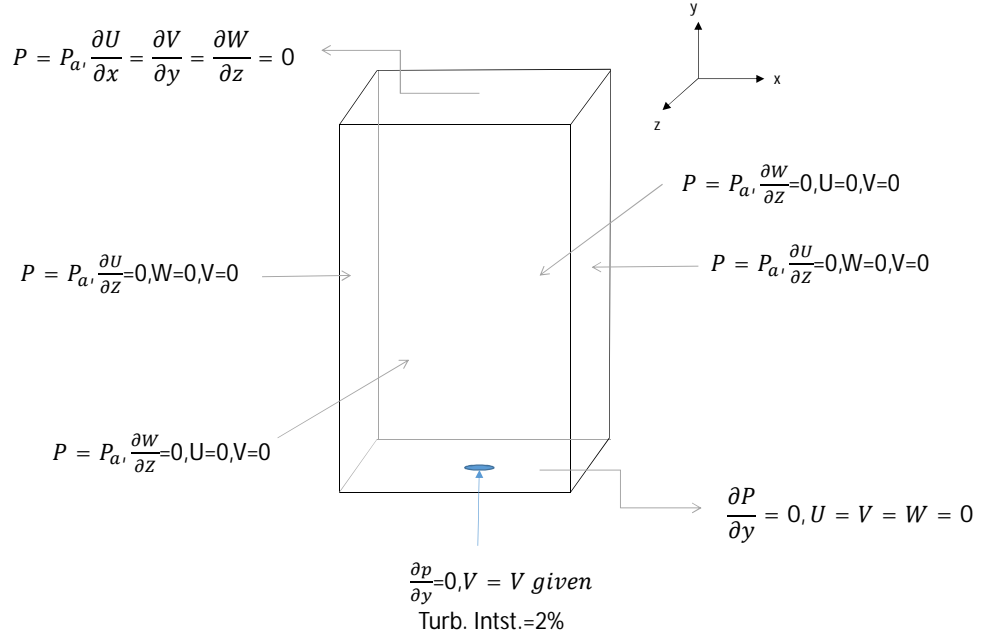


Figure 3.2: Schematic diagram of boundary conditions

## 3.2 Problem Definition

In this work two cases are simulated. the first one is where air is injected to a quiescent atmosphere of air. In the second one helium is injected to the quiescent atmosphere. The simulation works from these two cases were compared with the experimental results reported by Panchapakeshan and Lumley [2].

The problem which are considered in the thesis study is about axisymmetric jets issuing into quiescent air. For the air in air case the Reynolds number is taken to be 10,800 and for the helium jet the Reynolds number is taken as 4300. The flow is assumed to be incompressible, isothermal, average stationary and fully turbulent (high Reynolds number).

The flow parameters used in the air and helium cases are the same as reported by Panchapakeshan and Lumley [2]. Jet injection velocity and jet diameter are given in table 3.1. The fluid domain size of the air case is  $.6 * .6 * 1 \text{ m}^3$  ( $w * d * h$ ) which is

Case	Reynold's number	Jet velocity	Jet Diameter	Schmidt Number
Air	$1.1 * 10^4$	27m/s	6.1mm	0.7
Helium	$4.3 * 10^3$	72.5m/s	6.1mm	0.7

Table 3.1: Case Details

equivalent to  $100 * 100 * 170d_o^3$ , where  $d_o$  is the diameter at the inlet. The diameter is also taken as the characteristic length of all non-dimensional parameters calculated. The computational domain is taken in such a manner that it is large enough for predicting the farfield region. The Geometry considered for the present thesis work is shown in 3.3.

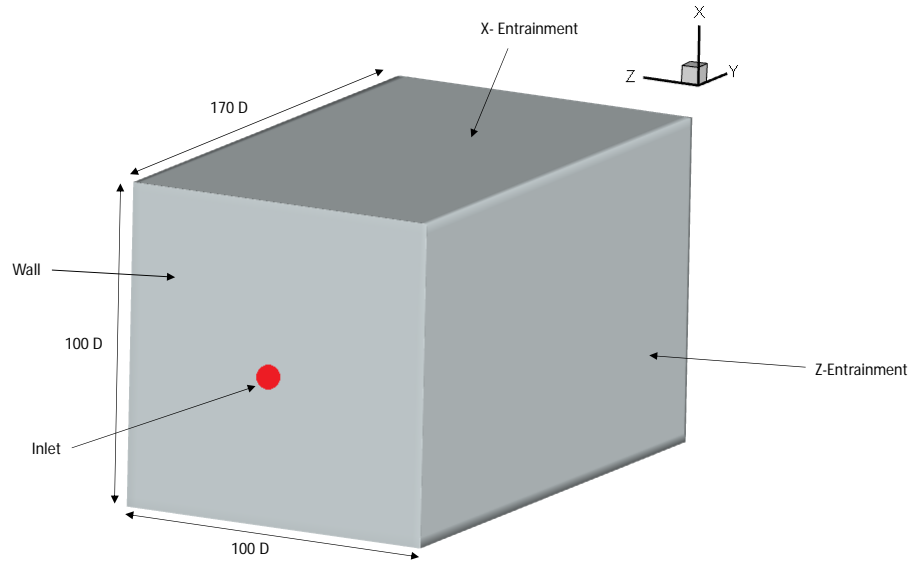


Figure 3.3: Computational Domain with geometric parameters.

### 3.3 Parallel Computing

Earlier CFD softwares were build using serial codes which were to be executed sequentially on one core or CPU. But in the modern era computers have mulyiple cores. So it was required to evelop solvers which utilizes the potential of all the CPUs. Computational requirement increases when number of grids is large, and higher order

schemes are implemented to reduce the numerical dispersion and dissipation. Also, validation and verification of the solver for cases involving complex geometries and larger computational domains turn time-consuming as grids having millions of cells need to be used. Both Direct Numerical Simulation (DNS) and Large Eddy Simulation (LES) turbulence modeling techniques, require very

fine meshes for capturing the eddies. Therefore parallelisation of code is required. A parallel program simultaneously uses more than one CPU to speed up computations where as a serial one uses a single CPU. This is done to increase the speed of computation. The development of high-performance clusters and super-computers have boosted the power of CFD.

Parallel CPUs are widely used in CFD to implement data-parallelism. These are broadly classified into two

- Single-Instruction Single-Datastream (SISD) systems
- Multiple-Instruction Multiple-Datastream (MIMD) systems

SISD systems support parallelism only at an operational level and are ineffective in problems which are very large. MIMD systems, on the other hand, consist of numerous autonomous processors, each processor being a full fledged CPU. Every CPU has its local clock and operate asynchronously. MIMD systems are of two types based on the memory accessible to its processors.

- Shared memory MIMDs
- Distributed memory MIMDs

Shared memory MIMDs have a collection of memory modules which are openly accessed by all the processors through an interconnection network. Processors simultaneously accessing the memory can saturate the network due to limited bandwidth. This architecture scales well only up to a fixed number of processors because of the extra cost incurred in creating high bandwidth interconnection networks. Distributed memory MIMDs, on the other hand, have a large number of nodes. A node refers to a processor and its individual memory module. Workstations, high-performance clusters, and supercomputers are built using this architecture. Message passing between independent processes running on various nodes is the main bottle-neck in such systems, in achieving linear speed-up in which the computation time scales as the reciprocal of the number of CPUs. Although nodes access their memory modules freely,

passing data between processors is often carried out along intersecting, or overlapping networks. A fully connected network in which each processor is connected to every other processor directly is too expensive.

### Shared Memory Parallelism

Shared memory parallel computing using open Multi-processing(OpenMP) or OpenACC are often used to speed up sections of a serial code. It is based on dynamic process creation and can be used even on distributed memory MIMDs by creating a global address space. It offers a relatively more straightforward implementation with minimum modification to the existing code. However, the main downside is that shared memory parallel programming cannot provide linear speedup as the code is still being executed in serial at critical sections. The level of parallelism is limited as processes may run different independent parts of the same code at any given point.

### Message Passing Interface(MPI)

MPI has become the most common and convenient way of programming distributed memory MIMDs. It can facilitate complete parallelism among processors in a system using explicit message passing across processes. It has open-source implementations like OpenMPI and MPICH, which can be used to parallelize any code written in C or Fortran. MPI can be used to program parallel codes either by dividing the data among processors known as data-parallel approach; or by partitioning large algorithms to execute on different processors known as control-parallel approach. The latter approach is preferred in case of codes that are smaller in size and uses coarser meshes. The scalability of an algorithm-parallel solver is limited to a

fixed number of processors depending on the size of the longest critical(serial) section in the code. Amdahl's law proposes that such a code run on any number of processors exceeding the scalable limit will lead to wastage of computational power. A natural way of overcoming the Amdahl's law barrier in scalability is to adopt a data-parallel approach. Hence, in the case of large CFD codes, the most prudent strategy is to distribute the computational domain among processes and execute the same code on each of these in parallel. Researches using MPI for parallelization face two main challenges which are

- Load balancing

- Achieving linear speedup

Efficient mesh partitioning software should be used to divide data maintaining continuity and minimizing common edges/interfaces. The load balancing part is crucial as the processor handling the largest amount of data in a poorly balanced system determines the computational time taken by all the processes in the system. The optimal case is the one in which each process handles an equal amount of data, given that all processors remain equally fast. Communicating information at the interfaces of partitions maintains continuity across the entire domain. It may seem initially that well-balanced data parallel programs can provide a speed-up equal to the number of independent processes used to run a program. The time taken for inter-process communication should be minimized by reducing the number of interface cells/nodes.

### 3.3.1 SMAC Algorithm

A CFD solver can either be explicit or implicit while performing the temporal integration of Navier-Stokes equation. An implicit solver is unconditionally stable of all  $\Delta t$  time step size. It requires an iterative method to solve the set of algebraic discretized equation. Therefore when the temporal timestep requirement is very small due to the underlying flow physics, DNS/LES turbulence modelling, implicit modelling becomes computationally expensive. on the otherhand explicit formulation of the temporal integration of the Navier Stokes equation results in a set of discretized equation that can be solved directly without resorting to the iterative methods. However explicit solver requires that explicit solver satisfy the CFL(Courant Frederick Lewis) criterion for numerical stability. For a convection term CFL requirement is satisfied when,

$$\Delta T_{convec} \left( \frac{|U|}{\Delta x} + \frac{|V|}{\Delta y} + \frac{|W|}{\Delta z} \right) \leq 1 \quad (3.29)$$

The diffusion term criteria requires,

$$\Delta T_{diffusion} \sigma \left( \frac{|U|}{\Delta x^2} + \frac{|V|}{\Delta y^2} + \frac{|W|}{\Delta z^2} \right) \leq \frac{1}{2} \quad (3.30)$$

$\sigma$  is equal to  $\mu/\rho$  for the momentum equation and  $D_{12}$  for the species mass fraction equation. The smallest of the above two  $\Delta t$  is taken as the time step size. Explicit scheme based on Marker and Cell method of Harlow and Welch[32] is used in work.

# Chapter 4

## Results and Discussion

This chapter is divided into two parts where at first the air in air case is discussed followed by the discussion of helium in air.

The simulations were performed using Dynamic k-equation model LES and the results had been compared with the experimental results. This simulation is used as a benchmark to ensure results[2]. The plume formation is shown in images. Time averaged velocity profiles have also plotted. Additionally the rms quantities of the fluctuating quantities and Reynolds stresses have been plotted.

### 4.1 Computational Grid

The geometry and mesh of the fluid domain was developed in ICEMCFD. The domain for computation consists of a cuboidal geometry. The geometry consists of an inlet orifice of 6.1mm diameter from where the jet enters, an outlet at 1m above the inlet, a wall and two entertainments in the x and z directions. The inlet part is very finely meshed and it is of the order of the kolmogorov length scale.

For proper resolution of the fluid dynamics, the computational grid is made non uniform by grading. The grading is specified in the directions where velocity gradients have higher value. The present case is an axisymmetric turbulent jet and the computational grid is graded in a manner to resolve axial velocity and lateral velocity gradients. Here we have two cases and one is the air in air case and the other is the helium in air case both are having different Reynolds number. Hence, the computational grid is smaller cells near the jet inlet. and near the jet axis. Based on the Kolmogorov's length scales two different meshes were made for obtaining the flow dynamics of both the cases which are the air in air case and the helium in air case. The

mesh used for air in air case is shown in 4.1. and the mesh used for helium in air case is shown in figure 4.2. The total cell count in the air case is  $1.1 * 10^6$  and for the helium case is  $1.2 * 10^6$ .

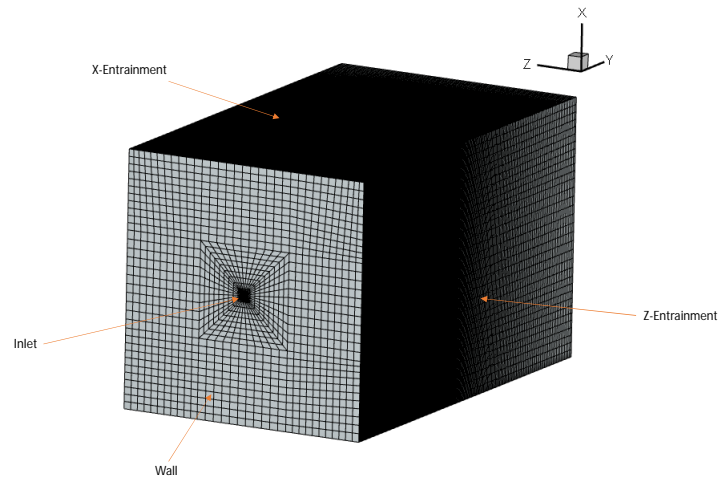


Figure 4.1: Computational Grid for air case

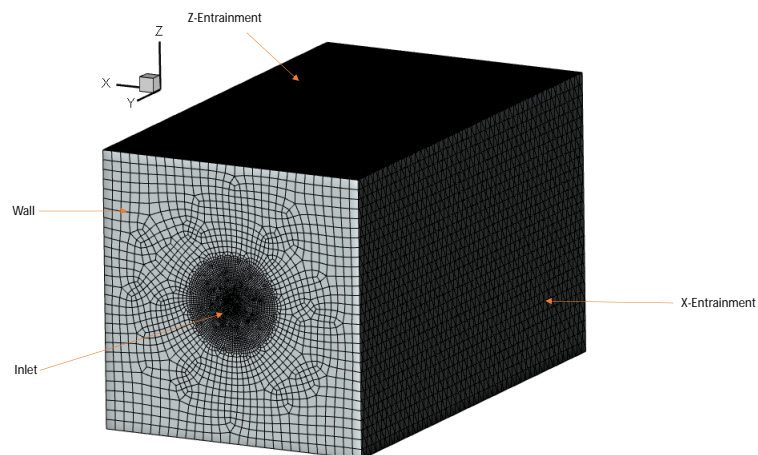


Figure 4.2: Computational grid with for helium case



## 4.2 Air in quiescent atmosphere

With the ability to resolve instantaneous flow fields in LES, numerical results of the turbulent intensities can be compared with the experimental observations.

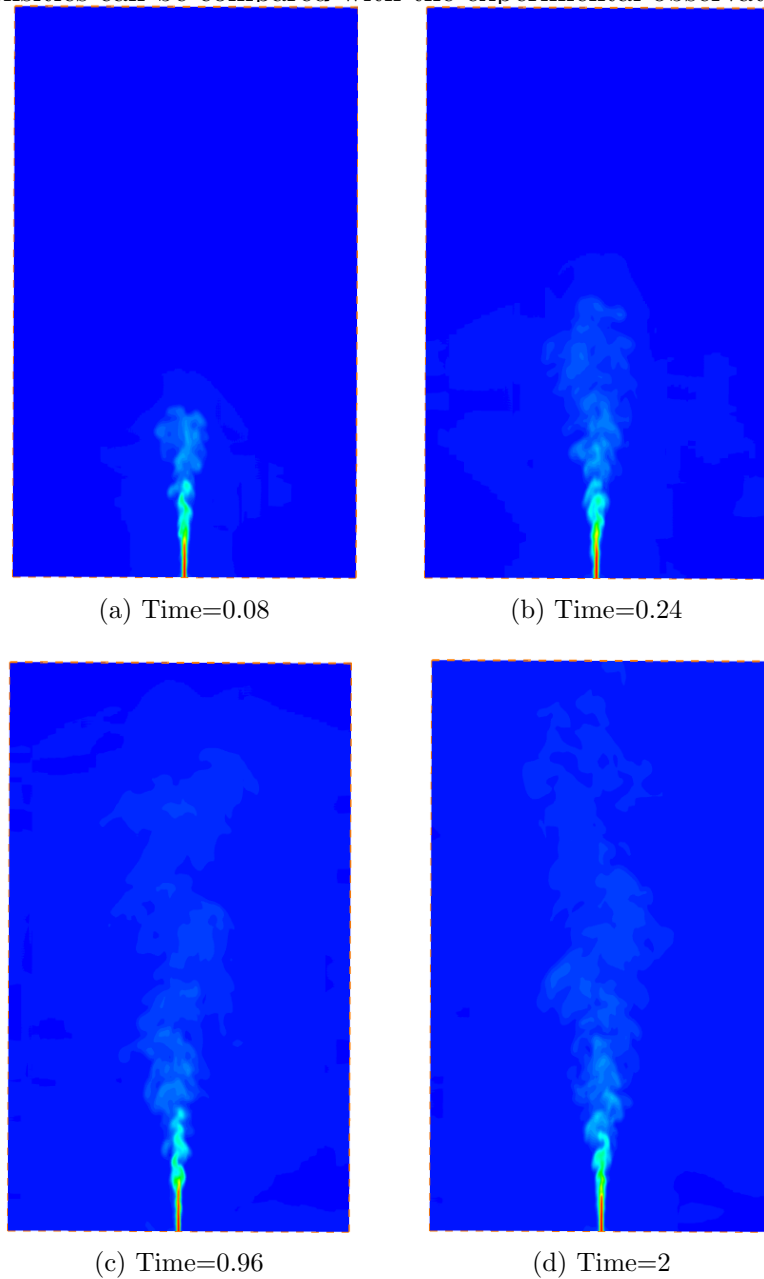


Figure 4.3: Mass fraction development of air jet at various time

All the post processing works are done using Tecplot 2009 and Origin 9 has been used for plotting the curves. The velocity with which the air enters the inlet orifice of 6.1 mm is taken to be 27m/s. The developmet of the air mass fraction has been shown in the following figures 4.3 at diffenert times from the beginning of the start

time. Here in the figures the development of the jet is shown clearly as how it spreads as it begins from the inlet.

The time averaged velocity profile is shown in the following figure 4.4. This is plotted after a time of 100 times the residence time. Here the variation of the mean of the velocity is done and the result is as expected. The profile image is captured by taking a mid plane of the mesh and slicing it. The resulting figure is shown at the mid place of the domain geometry.

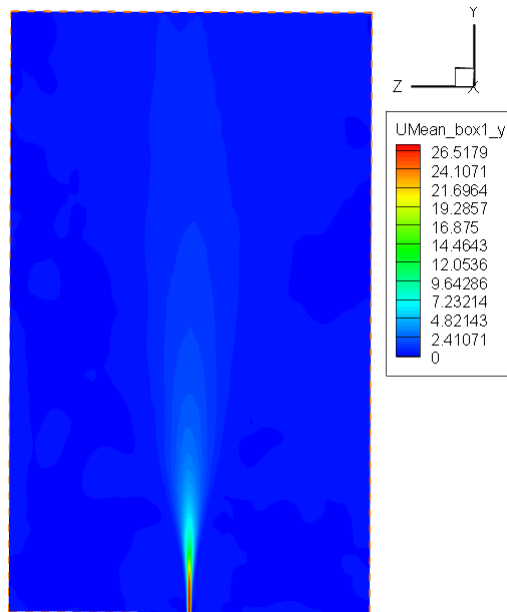


Figure 4.4: Mean Velocity profile

Now all the necessary analysis is discussed below. The variation of the axial mean velocity in the radial direction is shown in the figure 4.5. The obtained profile is very similar to the experimental result of Panchapakeshan and Lumley [2]. The image depicts a symmetry in the y axis. The maximum velocity at the centre and decreases along the radial direction. The measurement is taken in the far wake region at  $\frac{y}{d} = 0.4$ . The half width for the mean velocity profile, the value of  $\frac{r}{x}$  when  $\frac{U}{U_s} = 0.4$ , was 0.096. Integrating the mean velocity profile the ratio of mass flux at a section to the mass flux at the nozzle to be  $\frac{m}{m_0} = 0.32x/d$ . The time averaged mean velocity profile is plotted after the jet has passed 75 times the residence time and it has reached steady state. Residence time is actually the ratio of the axial distance to the initial velocity and its value is 0.034s. The plot which justifies this is provided in the plot 4.6, which shows the variation of velocity at the point with time.

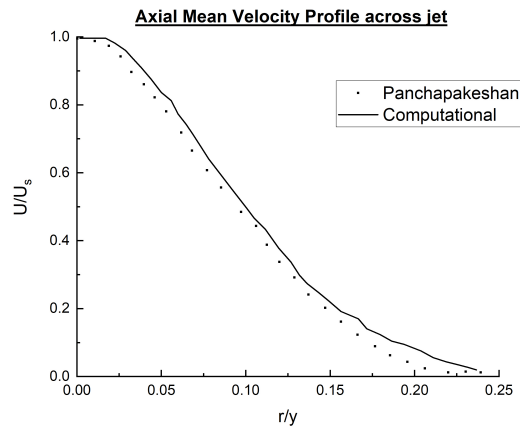


Figure 4.5: Axial Mean Velocity profile in the radial direction

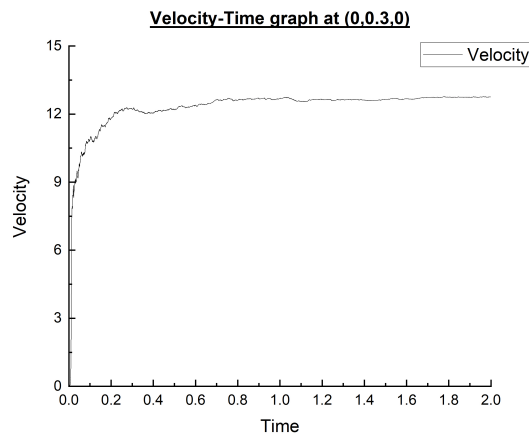


Figure 4.6: Velocity variation with time at (0,0.3,0)

The turbulent intensities in the axial, radial and azimuthal directions are shown in the following figures. The turbulent intensity variation in the axial direction is shown in figure 4.7. There is an off axis peak observed in the axial turbulent intensity. This is not clearly observed in other measurements in the far field, but has always been seen in the near field, close to the nozzle. The peak is expected to be because of the shear production of kinetic energy which has a distinct off axis peak at nearly the same location.

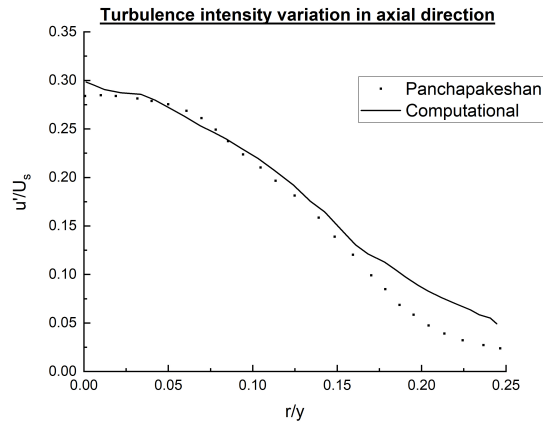
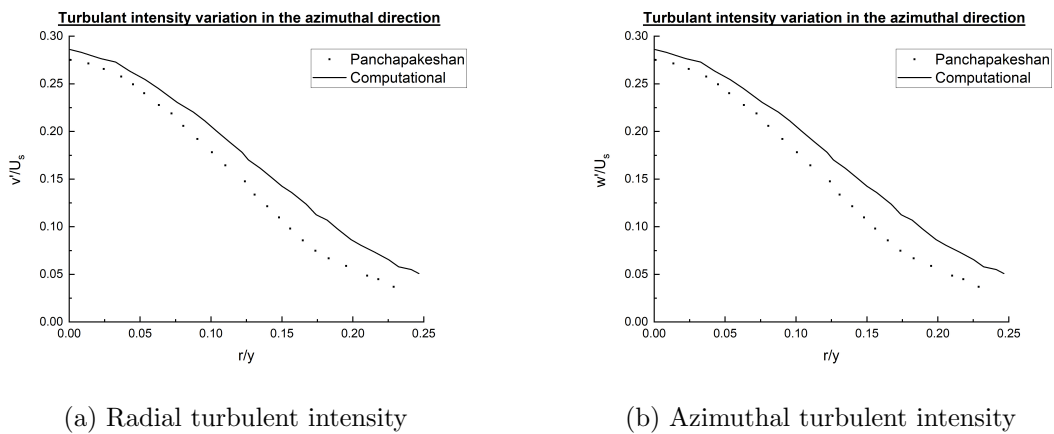


Figure 4.7: Axial Turbulent intensity variation in the radial direction

The turbulent intensity variations in the radial and azimuthal directions show similar variation as the jet is symmetric as shown in figure 4.8 . Both the intensity plots are in agreement with the experimental result of Lumley and Panchapakeshan[2].



(a) Radial turbulent intensity

(b) Azimuthal turbulent intensity

Figure 4.8: Radial and Azimuthal Turbulent intensity variation in the radial direction

The Reynolds stress variation along the radial direction is shown in figure 4.9. In fluid dynamics, the Reynolds stress is the component of the total stress tensor in a fluid obtained from the averaging operation over the Navier–Stokes equations to account for turbulent fluctuations in fluid momentum. Any changes in the Reynolds Stresses will affect the velocity field. For example in Jets, it can alter the velocity decay or spread rate. Though it's not a true stress (it's a flow property), it reflects the effects of the momentum fluxes induced by the turbulence. They actually represent the degree of the momentum exchange at a given point in the flow. They can also be

perceived as a conduit for transferring energy from mean flow to the turbulence. The obtained profile for the Reynolds stress is over predicted in the present simulation result as it had slight over prediction the other intensity values. Here in the obtained profile there is an off axis peak for the Reynolds stresses. But still the trend in the variation is the same.

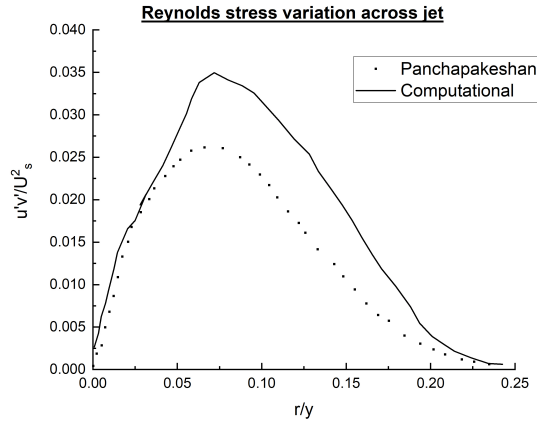


Figure 4.9: Axial Turbulent intensity variation in the radial direction

In this work, energy spectrum analysis is used to justify the adequacy of grid instead of grid independence.

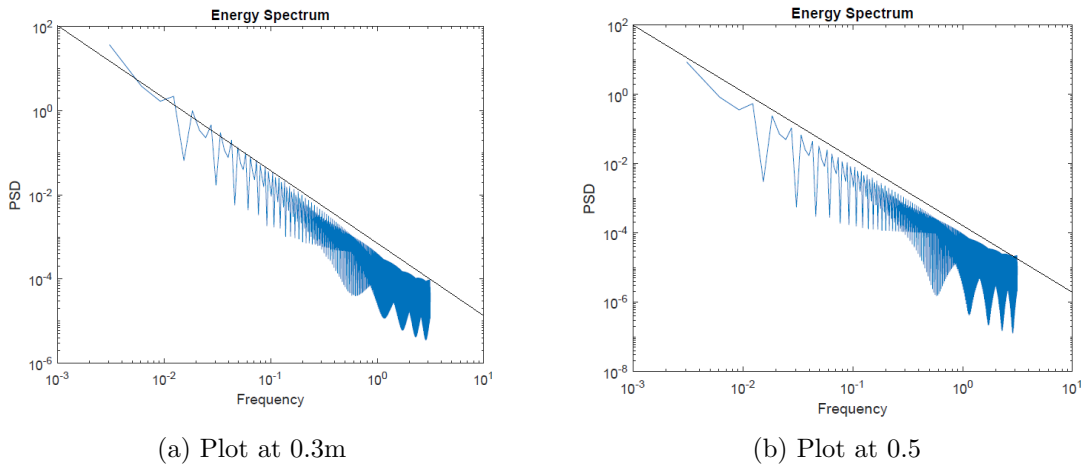


Figure 4.10: Energy Spectrum

The velocity spectra has been plotted at two different locations for the present simulation, one is at  $y=0.3\text{m}$  and the other at  $y=0.5\text{m}$ . The black line represents the  $-5/3$  slope of the Kolmogorov Spectrum. The code has been written and the graphs

are plotted in Matlab. The plots have been shown in figure 4.10. As can be seen from the plots the energy spectrum of the two locations have a slope of  $-5/3$  and the grid used in this simulation captures the flow dynamics upto the inertia scale and hence suitable for LES simulation.

## 4.3 Running Parallel Applications

Parallel computing method used by openFoam is called domain decomposition in which the geometry and associated fields are broken into several pieces and allocated to separate processors for solution. The processes involved in parallel computation are decomposition of mesh and fields, running the application in parallel and post-processing the decomposed case. The parallel running uses the public domain openMPI implementation of the standard message passing interface (MPI) by default, although other libraries can be used.

The mesh and fields are decomposed using the *decomposePar* utility. The underlying aim is to break up the domain with minimal effort but in such a way to guarantee an economic solution. The geometry and fields are broken up according to a set of parameters specified in a dictionary named *decomposeParDict* that must be located in the system directory of the case of interest.

Here in the present research we have done the domain decomposition using two methods which are:

- Simple
- Scotch

### Simple

Simple geometric decomposition in which the domain is split into pieces by direction, e.g. 2 pieces in the x direction, 1 in y etc. The plot for comparison of the time of simulation for 100 timesteps using scotch and Simple is shown in the figure 4.11. Along with that a comparison of the speed up of the theoretical and actual processor is shown in the figure 4.11. The value of speedup is taken as an inverse of time as speed is inversely proportional to time.

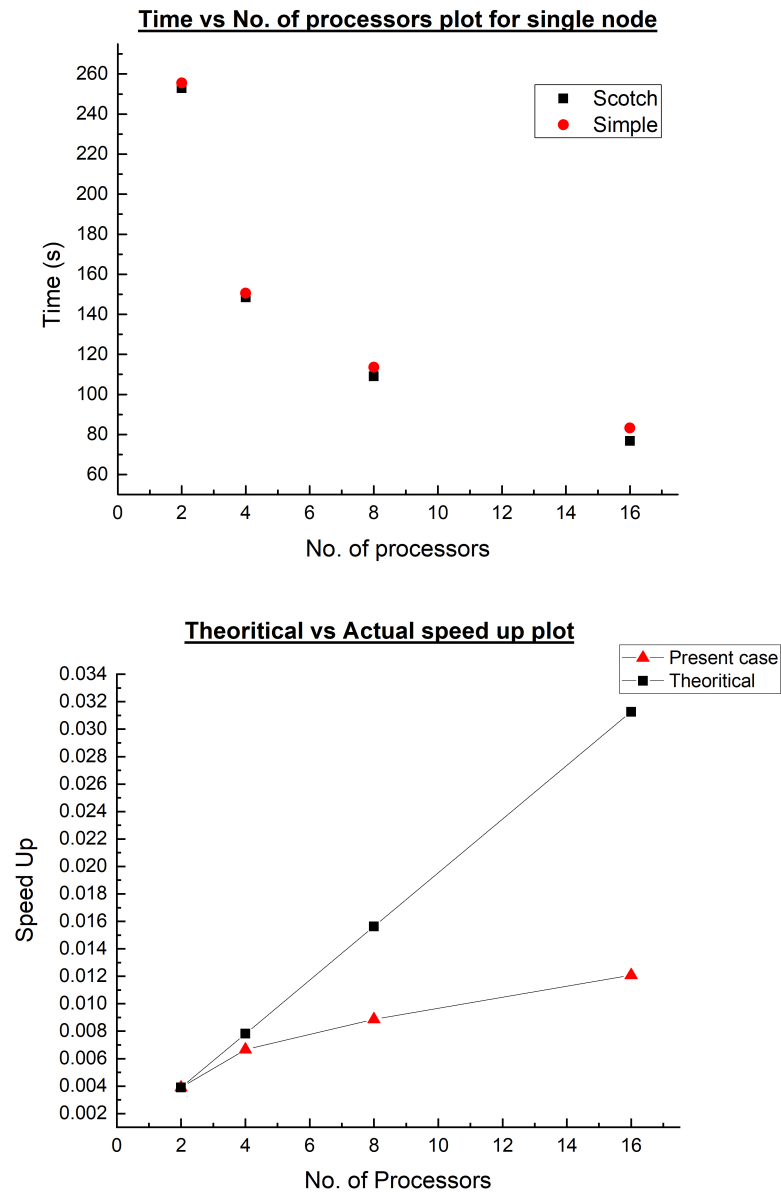


Figure 4.11: (a)Time vs No. of processors plot(b)Actual vs Theoretical Speed up plot

### Scotch

Scotch decomposition does not require any geometric input from the user and attempts to minimise the number of processor boundaries. The user can specify a weighting for the decomposition between processors, through an optional processor-Weights keyword which can be useful on machines with differing performance between processors. There is also an optional keyword entry strategy that controls the decomposition strategy through a complex string supplied to Scotch.

A comparison of the time required for the execution of the simulation was done by the above mentioned techniques using 2,4,8 and 16 processors in the same node for 100 iterations as shown in the figure 4.11 .

From the plot conclusion is made which is that both the simple and scotch techniques were comparable to each other. Also it is evident that time required for simulation is less using 16 processors. So all the simulations were done using 16 processors.

## 4.4 Helium into quiescent atmosphere

This section comprises the second part of the thesis work. Here a high density ratio plume is simulated, where the density ratio defined as the ratio between density of air to that of helium. Experimental works had been done by Lumley and Panchapakeshan [19] as a second part of their research work. To investigate movement of helium plume a 3D mesh with a time dependent study using the Large Eddy Simulation (LES) approach is undertaken. In addition to the averaged quantities, rms quantities are also investigated for proper understanding of the plume dynamics. An LES subgrid model of Dynamic k Equation is taken as the turbulence model in the present simulation. All the codes are done in openFoam and the results are investigated using Tecplot and the graphs are plotted using Origin 9. According to the experiments done they have used the same experiment setup for the investigation of the helium jet. So the same geometry is used and the mesh size has been re distributed as a finer mesh is made in accordance with the kolmogorov length scale to capture the turbulent parameters.

So the same geometry is used and the mesh size has been re distributed as a finer mesh is made in accordance with the kolmogorov length scale to capture the turbulent parameters. The orifice diameter is taken to be 6.12mm and the velocity of the helium is taken as 72.5m/s. The plume inlet is located at the center of the bottom plane. From both the entrainments air is flowing towards the jet flow.



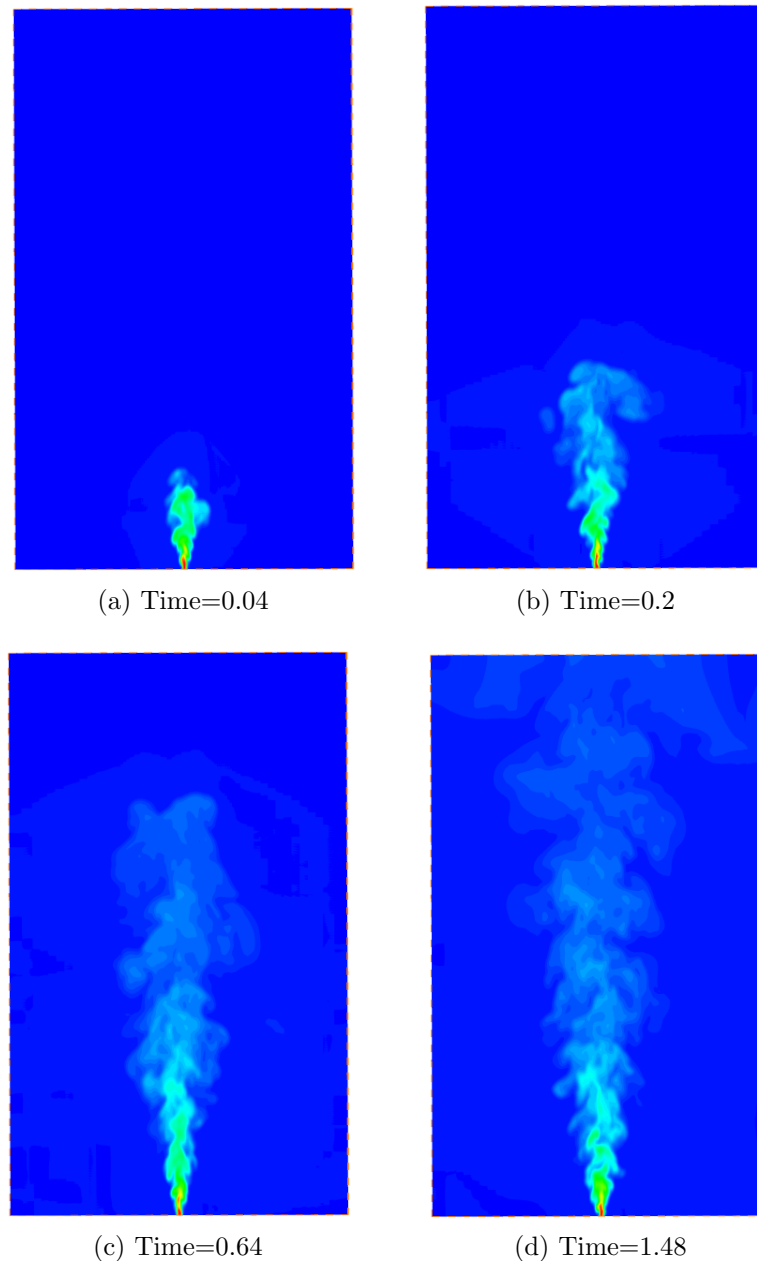


Figure 4.12: Mass fraction development of helium jet at various time

The development of the air mass fraction has been shown in the following figures 4.12 at different times from the beginning of the start time. Here in the figures the development of the jet is shown clearly as how it spreads as it begins from the inlet. It is evident from the figures that the spreading is more compared to the air jet. When the low density helium gas enters the domain, it accumulates under a layer of higher density ambient air. The plume gas gathers until it generates a Rayleigh-Taylor instability. This is caused when a lighter fluid underlying a heavy fluid is accelerated. The

lighter gas gets accelerated upwards through the overlying fluid creating a toroidal vortex. The rising accelerating vortex entrains the surrounding air below it creating another heavy layer and the cycle repeats.

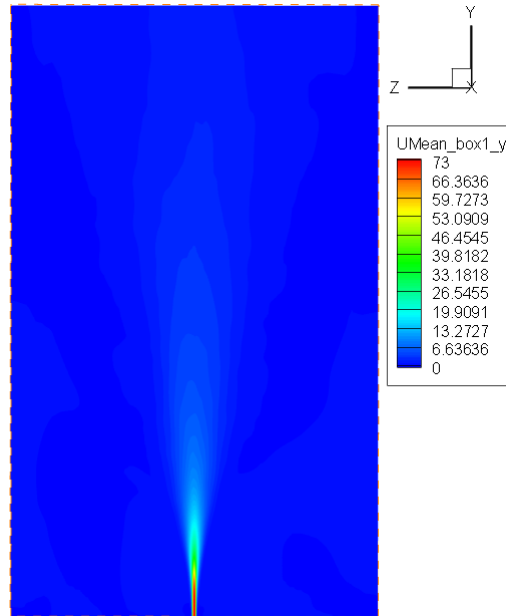


Figure 4.13: Mean velocity profile in the radial direction

The mean velocity profile is shown in figure 4.13. Here the variation of the mean of the velocity is done and the result is as expected. The profile image is captured by taking a mid plane of the mesh and slicing it. The resulting figure is shown at the mid place of the domain geometry. The time averaged mean velocity profile is plotted after the jet has passed 80 times the residence time and it has reached steady state. The plot which justifies this is provided in the plot 4.14, which shows the variation of velocity at the point with time. The mean velocity profile in the radial direction is shown in figure 4.15. The obtained profile is very similar to the experimental result of Panchapakshan and Lumley [19]. The image depicts a symmetry in the y axis. The profile is plotted at the location where  $\frac{y}{d} = 90$ .

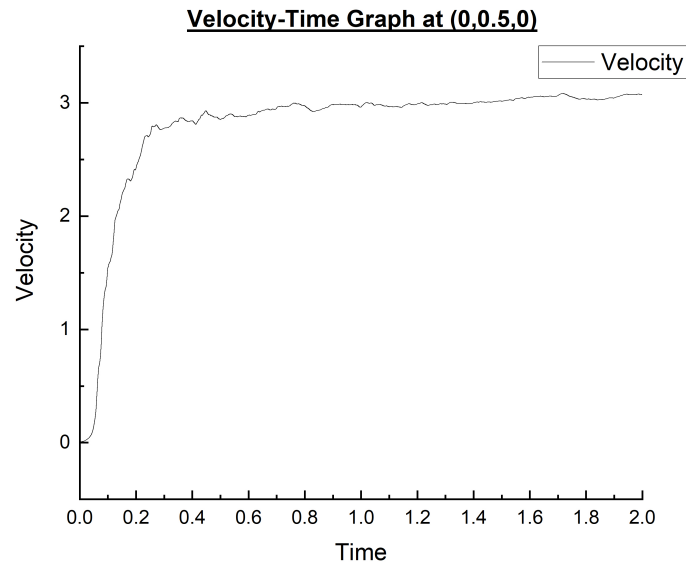


Figure 4.14: Variation of velocity at (0,0.5,0)

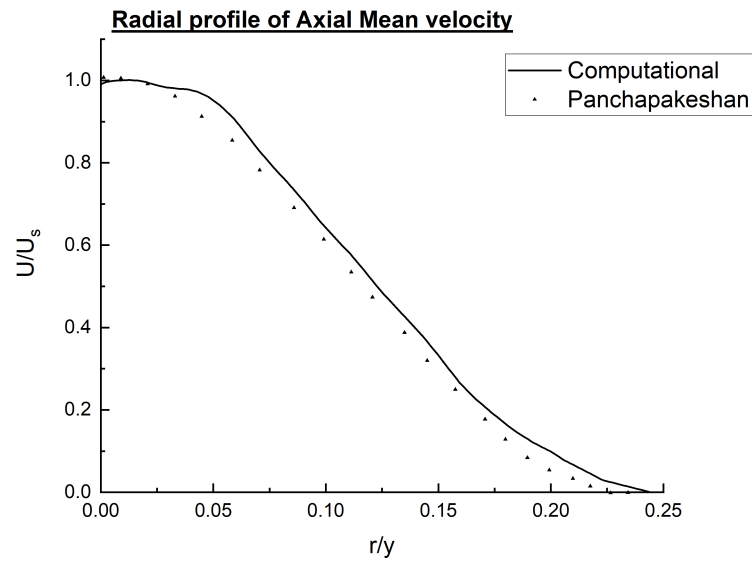


Figure 4.15: Velocity profile in the radial direction

The axial turbulent intensity variation in the radial direction is shown in the figure 4.16 .The simulated result is overpredicted but the trend in the graph is similar to the experimental result.

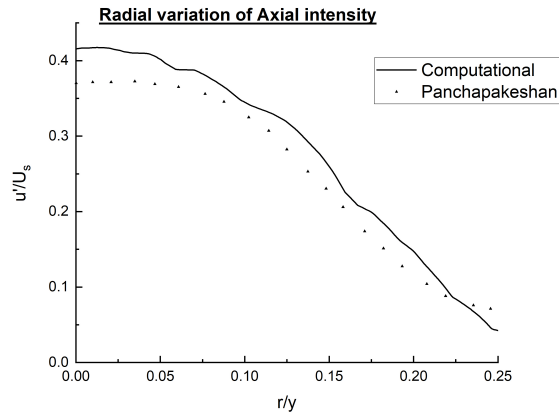
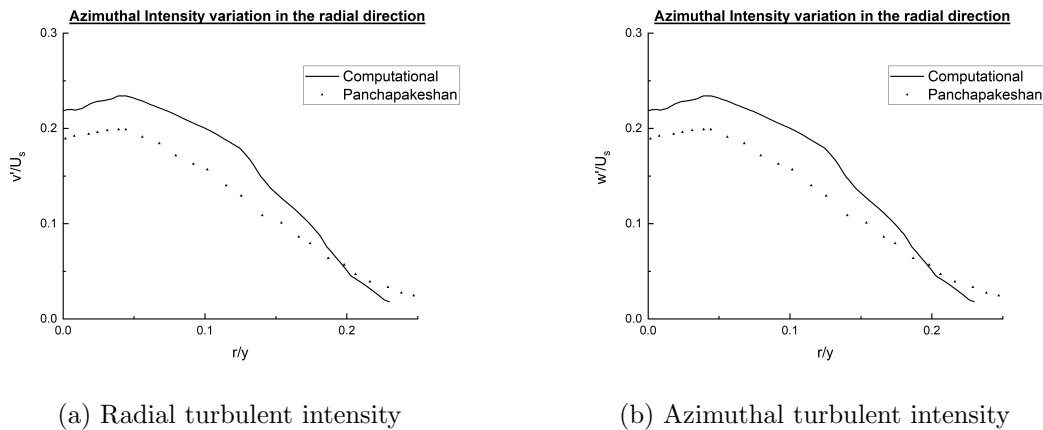


Figure 4.16: Mean velocity profile in the radial direction

The turbulent intensities of azimuthal and radial velocity fluctuations along the axis of the jet are shown in figure 4.17.



(a) Radial turbulent intensity

(b) Azimuthal turbulent intensity

Figure 4.17: Radial and Azimuthal Turbulent intensity variation in the radial direction

The intensity of axial velocity fluctuations are almost twice as large as the radial and azimuthal components. In comparison with the values measured in the air jet, the axial velocity fluctuations are about 80% to 90% larger while the radial intensities are of about the same order. This wide range for their flow configuration is very close to the plume region. The profiles for intensities of azimuthal and radial velocity fluctuations in the helium jet are virtually identical with those for the air jet. The intensity of axial velocity fluctuations, as mentioned earlier, is higher than the air jet values in the fully turbulent region near the axis of the jet. The intensity values are somewhat

over predicted but the trend in the graphs are similar to the observed experimental results.

The Reynolds stress variation across the helium jet is shown in the figure 4.18.

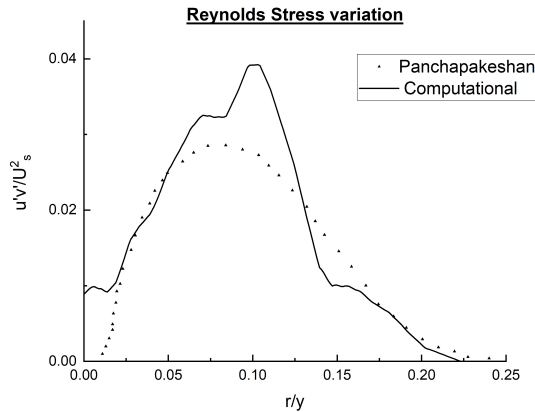


Figure 4.18: Reynolds stress variation across the helium jet

The values for the helium jet are higher near the peak than for the air jet, but towards the edge of the jet both agree well with each other. The mean velocity decay along the axis agrees with the scaling indicated by the effective diameter. The radial profile of mean velocity is wider than that for the air jet, a consequence of the mean momentum added by the buoyancy. The spreading rates of the mean velocity and concentration fields indicate a turbulent Schmidt number of 0.7, which agrees with other measurements of scalars in round jets. Significantly higher levels of axial velocity turbulent intensities are observed. It is believed that the origins of these higher levels must lie in the near-field development of the jet, a region not studied in the present investigation.

Here in the present research instead of the grid independent test the Energy spectrum method is plotted as explained in the theory chapter. As mentioned in the above section there are specific quality parameters to check the suitability of the grid for large eddy simulation. One of the parameters of such is the Energy Spectrum plot. The velocity spectra has been plotted at two different locations for the present simulation. The black line represents the  $-5/3$  slope of the Kolmogorov Spectrum. The code has been written and the graphs are plotted in Matlab. The plots have been shown in figure 4.19.

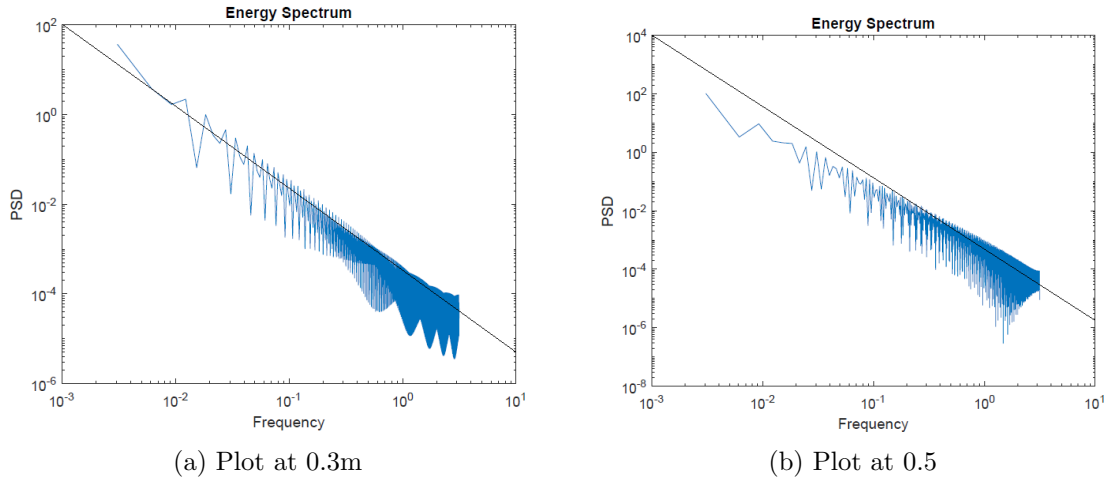


Figure 4.19: Energy Spectrum

The buoyancy driven turbulence emerging from the small scales of motion is not resolved adequately in the present implementation of LES. This could be an explanation of the over predictness of the turbulent fluctuations as shown in the present study. Moving away from the jet source the flow should get more and more turbulent due to shear production and buoyancy but the rate at which it does is higher than the experimental plume. Thus the turbulent intensity values and the reynolds stresses are over predicted and the plume rises with much lateral dissipation. The under resolved buoyancy induced turbulence is one likely cause for the over prediction of concentration values on the center axis since mixing rates of ambient fluid into the plume would be suppressed. Time averaged values for the two velocity components and the plume concentration showed little sensitivity to the mesh spacing.

## 4.5 CoVo Test

This test is done to check the compatability of the schemes which have been used in the above two cases. This test is basically the convection of a vortex on a constant, mean velocity flow. It represents the simplest prototype of what high fidelity codes must do in DNS or LES: convect vortices over long distances at the right speed and the right amplitude. Here we are not considering viscosity and the simulation basically expects the solution to be simple with the initial vortex which is convected along the mean flow. The computation is performed in a periodic box which means the boundary conditions are cyclic in all the faces. Comparing the solution at these

instants with the initial solution is an excellent qualification of the solvers accuracy.

The schematic of the case is given by the figure 4.20. A 80\*80 grid is used for the simulation in this case.

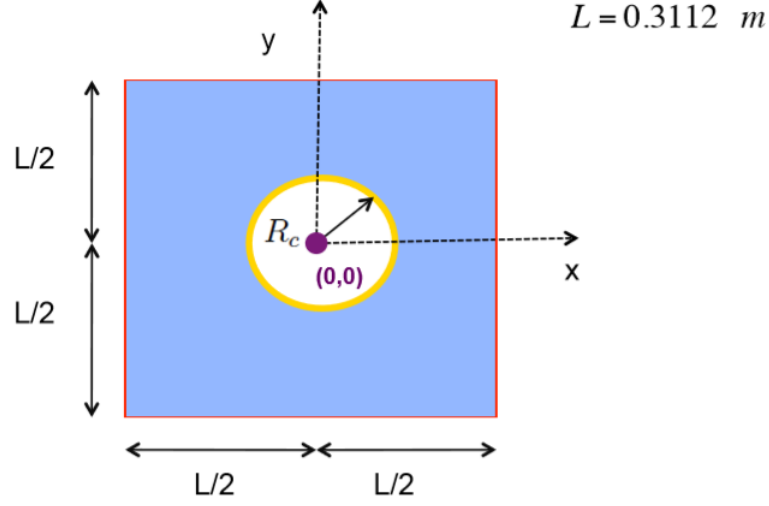


Figure 4.20: Geometry for CoVo test

The governing equations are given by the following equations,

$$u = U_o + \frac{\partial \Psi}{\partial y} \quad (4.1)$$

$$v = -\frac{\partial \Psi}{\partial x} \quad (4.2)$$

$$\Psi = \Gamma e^{-\frac{(x-x_o)^2 + (y-y_o)^2}{2R_c^2}} \quad (4.3)$$

$$p - p_o = -\frac{\rho \Gamma^2}{2R_c^2} e^{-\frac{(x-x_o)^2 + (y-y_o)^2}{R_c^2}} \quad (4.4)$$

$$U_o = 35m/s, \rho = 1.17kg/m^3, R_c = 0.01556m, \Gamma = 0.0036 \quad (4.5)$$

Here we are specifying a periodic boundary condition. So it is done by implimenting cyclic boundary condition in openfoam. The schematic of the boundary condition is given by the figure 4.21.

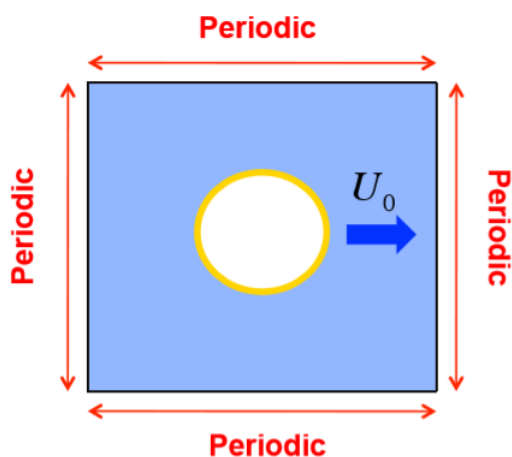


Figure 4.21: Boundary Condition for CoVo test

Here a non uniform initial condition had to be specified. That has been done by using a MATLAB code where the areas of the non uniform field is taken and specifying the initial non uniform conditions for pressure and velocities. Later with the values obtained to the corresponding cells the initial condition is implemented in openFoam. The initial conditions for velocity  $U_x$  and pressure are shown as in the figures 4.22 .

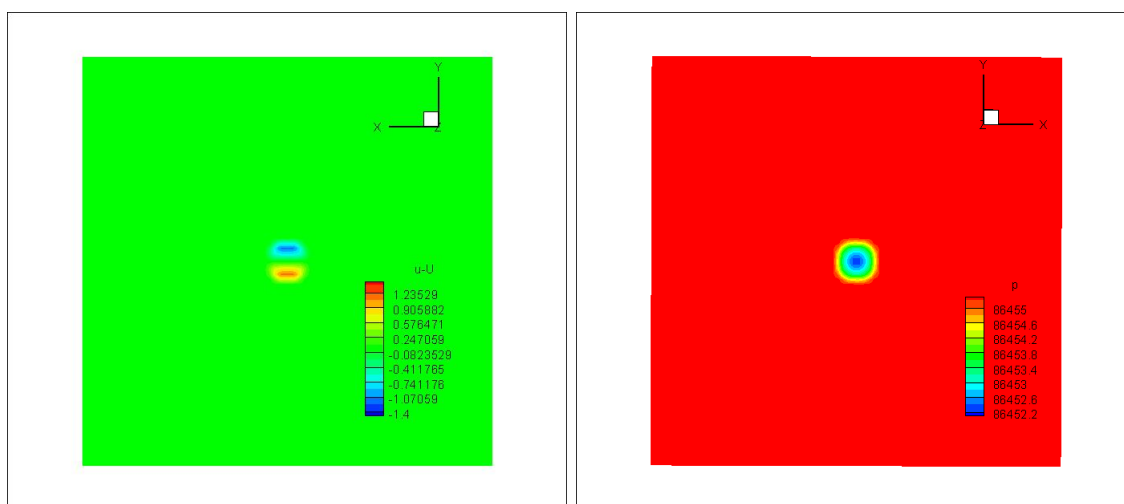


Figure 4.22: (a)Initial condition for  $U_x$  (b)Initial condition for Pressure

The result of the  $U_x$  after  $30\frac{L}{U}$  is shown in the figure 4.23.



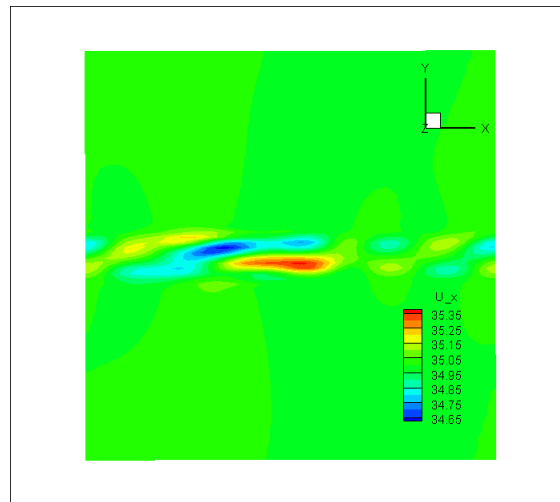


Figure 4.23:  $U_x$  image after  $30 \frac{L}{U}$  s

The plot of  $u - U$  vs  $x$  is shown in the figure 4.24. The schemes which the present work are second order accurate, while they have used fourth order accurate schemes, whereby the results are differing a bit. By the case we can mostly rely on the numerical schemes which we have used in our case.

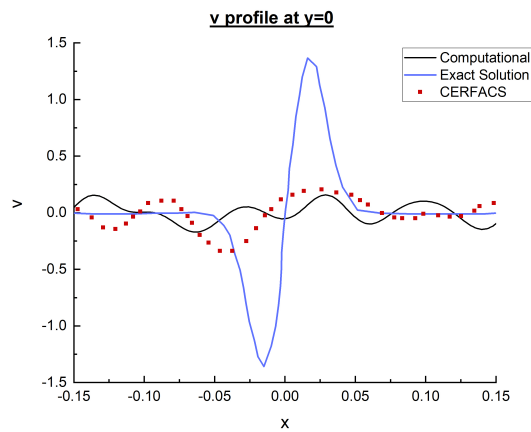


Figure 4.24: Plot of velocity in the  $y$  direction to  $x$

# Chapter 5

## Conclusions and Future Scops

The following conclusions have been made based on the results we have got.

Turbulent transport plays a dominant role in the energetics of many flows and it is important to account for it accurately in any prediction scheme. The mean velocity decay along the axis agrees with the scaling indicated by the effective diameter for both the cases ie the air in air case and the helium in quiscent air. The radial mean velocity profile of helium jet is wider than that for the air jet, a consequence of the mean momentum added by the buoyancy. Significantly higher levels of axial velocity turbulent intensities are observed. It is believed that the origins of these higher levels must lie in the near-field development of the jet, a region not studied in the present investigation. The verasatality of Openfoam was also understood compared to other CFD softwares. Being an opensource software it is of free of cost. Most importantly we can customise the codes based on out necessities. Also the efficiency of LES is also learned as it is much superior in giving results of instantaneous values. It makes a significant alternative to Direct Numerical Simulations especially for modelling turbulence flows.

Future work is basically to add mixture fraction equations to the existing solver and have a solver for combustion. A flamelet based model can be incorporated in the existing solver. The chemistry in the solver can be controlled using openFoam so does the combustion properties.

# References

- [1] W. Rodi. Turbulent Buoyant Jets and Plumes: HMT: The Science & Applications of Heat and Mass Transfer. Reports, Reviews & Computer Programs, volume 6. Elsevier, 2014.
- [2] N. Panchapakesan and J. Lumley. Turbulence measurements in axisymmetric jets of air and helium. Part 1. Air jet. *Journal of Fluid Mechanics* 246, (1993) 197–223.
- [3] M. Nived and V. Eswaran. Parallelization of a Hybrid Unstructured Grid Density-based Flow Solver. Ph.D. thesis, Indian institute of technology Hyderabad 2018.
- [4] E. Marotta. Fire losses in Canada. *Council of Canadian Fire Marshals and Fire Commissioners, Ottawa, ON* .
- [5] L. F. Richardson. Weather prediction by numerical process. Cambridge University Press, 2007.
- [6] A. N. Kolmogorov. The local structure of turbulence in incompressible viscous fluid for very large Reynolds numbers. *Cr Acad. Sci. URSS* 30, (1941) 301–305.
- [7] J. Smagorinsky. General circulation experiments with the primitive equations: I. The basic experiment. *Monthly weather review* 91, (1963) 99–164.
- [8] D. K. Lilly. A proposed modification of the Germano subgrid-scale closure method. *Physics of Fluids A: Fluid Dynamics* 4, (1992) 633–635.
- [9] J. W. Deardorff. Numerical investigation of neutral and unstable planetary boundary layers. *Journal of the Atmospheric Sciences* 29, (1972) 91–115.
- [10] M. Germano, U. Piomelli, P. Moin, and W. H. Cabot. A dynamic subgrid-scale eddy viscosity model. *Physics of Fluids A: Fluid Dynamics* 3, (1991) 1760–1765.

- 
- [11] T. Cebeci. Analysis of turbulent boundary layers, volume 15. Elsevier, 2012.
- [12] P. Spalart and S. Allmaras. A one-equation turbulence model for aerodynamic flows. In 30th aerospace sciences meeting and exhibit. 1992 439.
- [13] F. Nicoud and F. Ducros. Subgrid-scale stress modelling based on the square of the velocity gradient tensor. *Flow, turbulence and Combustion* 62, (1999) 183–200.
- [14] G. Kumar, S. Lakshmanan, H. Gopalan, and A. De. Investigation of the sensitivity of turbulent closures and coupling of hybrid RANS-LES models for predicting flow fields with separation and reattachment. *International Journal for Numerical Methods in Fluids* 83, (2017) 917–939.
- [15] R. Soni, N. Arya, and A. De. Characterization of turbulent supersonic flow over a backward-facing step. *AIAA Journal* 1511–1529.
- [16] A. Kravchenko and P. Moin. On the effect of numerical errors in large eddy simulations of turbulent flows. *Journal of computational physics* 131, (1997) 310–322.
- [17] B. J. Geurts and J. Fröhlich. A framework for predicting accuracy limitations in large-eddy simulation. *Physics of fluids* 14, (2002) L41–L44.
- [18] N. Arya and A. De. Effect of grid sensitivity on the performance of wall adapting SGS models for LES of swirling and separating–reattaching flows. *Computers & Mathematics with Applications* .
- [19] N. Panchapakesan and J. Lumley. Turbulence measurements in axisymmetric jets of air and helium. Part 2. Helium jet. *Journal of Fluid Mechanics* 246, (1993) 225–247.
- [20] K. B. McGrattan, H. R. Baum, and R. G. Rehm. Large eddy simulations of smoke movement. *Fire Safety Journal* 30, (1998) 161–178.
- [21] T. Ma and J. Quintiere. Numerical simulation of axi-symmetric fire plumes: accuracy and limitations. *Fire Safety Journal* 38, (2003) 467–492.
- [22] X. Zhou, K. Luo, and J. Williams. Study of density effects in turbulent buoyant jets using large-eddy simulation. *Theoretical and Computational Fluid Dynamics* 15, (2001) 95–120.

- 
- [23] T. O’hern, E. Weckman, A. Gerhart, S. Tieszen, and R. Schefer. Experimental study of a turbulent buoyant helium plume. *Journal of Fluid Mechanics* 544, (2005) 143–171.
- [24] P. E. DesJardin, T. J. O’Hern, and S. R. Tieszen. Large eddy simulation and experimental measurements of the near-field of a large turbulent helium plume. *Physics of fluids* 16, (2004) 1866–1883.
- [25] B. Kannan. Computation of an axisymmetric jet using OpenFOAM. *Procedia Engineering* 127, (2015) 1292–1299.
- [26] B. E. Launder and D. B. Spalding. The numerical computation of turbulent flows. In *Numerical prediction of flow, heat transfer, turbulence and combustion*, 96–116. Elsevier, 1983.
- [27] H. Versteeg and W. Malalasekera. Computational fluid dynamics. *The finite volume method* .
- [28] M. Annarumma, J. Most, and P. Joulain. On the numerical modeling of buoyancy-dominated turbulent vertical diffusion flames. *Combustion and Flame* 85, (1991) 403–415.
- [29] L. Davidson. Second-order corrections of the k- $\varepsilon$  model to account for non-isotropic effects due to buoyancy. *International Journal of Heat and Mass Transfer* 33, (1990) 2599–2608.
- [30] F. M. White and I. Corfield. *Viscous fluid flow*, volume 3. McGraw-Hill New York, 2006.
- [31] J. Blazek. *Computational fluid dynamics: principles and applications*. Butterworth-Heinemann, 2015.
- [32] F. H. Harlow and J. E. Welch. Numerical calculation of time-dependent viscous incompressible flow of fluid with free surface. *The physics of fluids* 8, (1965) 2182–2189.